Journal Pre-proofs

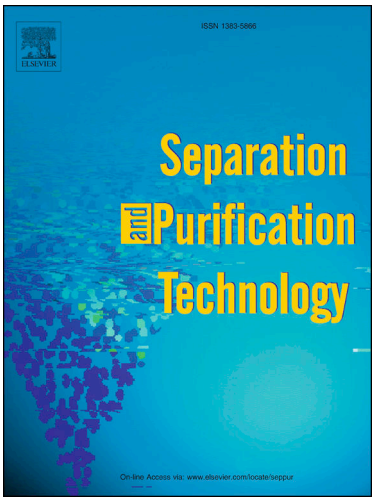

Solvent extraction in non-ideal eutectic solvents – application towards lanthanide separation

Ueslei G. Favero, Nicolas Schaeffer, Helena Passos, Kaíque A. M. L. Cruz, Duarte Ananias, Sandrine Dourdain, Maria C. Hespanhol

PII: S1383-5866(23)00500-2
DOI: https://doi.org/10.1016/j.seppur.2023.123592
Reference: SEPPUR 123592

To appear in: *Separation and Purification Technology*

Received Date: 27 January 2023
Revised Date: 1 March 2023
Accepted Date: 10 March 2023

Please cite this article as: U.G. Favero, N. Schaeffer, H. Passos, K. A. M. L. Cruz, D. Ananias, S. Dourdain, M.C. Hespanhol, Solvent extraction in non-ideal eutectic solvents – application towards lanthanide separation, *Separation and Purification Technology* (2023), doi: https://doi.org/10.1016/j.seppur.2023.123592

Solvent extraction in non-ideal eutectic solvents – application towards lanthanide separation

Ueslei G. Favero,† Nicolas Schaeffer,‡* Helena Passos,‡ Kaíque A. M. L. Cruz,† Duarte Ananias,‡ Sandrine Dourdain, Maria C. Hespanhol†*

† Group of Analysis and Education for Sustainability (GAES), Chemistry Department, Federal University of Viçosa (UFV), Viçosa, MG 36570–900, Brazil.

‡ CICECO - Aveiro Institute of Materials, Department of Chemistry, University of Aveiro, 3810-193 Aveiro, Portugal.

 Institut de Chimie Séparative de Marcoule, ICSM, CEA, CNRS, ENSCM, Univ Montpellier, BP 17171, Marcoule, 30207, Bagnols-sur-Cèze, France

* Corresponding email: mariacarmo@ufv.br; nicolas.schaeffer@ua.pt

ABSTRACT

Hydrophobic eutectic solvents (HES) emerged as promising substitutes to the conventional organic phase used in the solvent extraction (SX) of metal ions due to the avoidance of diluents and the suppression of third-phase manifestation. However, HES present a highly structured liquid phase defined by hydrogen-bonded interactions such that intercomponent interactions are expected to play a greater role in SX using HES compared to a diluted extractant solution. In this work, the extraction of lanthanides from nitrate media by the non-ideal solvent composed of decanoic acid ($C_{10}OOH$) and trioctylphosphine oxide (TOPO) was determined as a function of the lanthanide cation selection, HES molar fraction, HNO_3 concentration, and temperature. Through the systematic variation of these parameters, the delicate balance between complexation and solvent reorganisation and its influence on the extraction and metal selectivity is determined by metal partition experiments, time resolved fluorescence and Raman spectroscopy, and small-angle X-ray scattering (SAXS). A compromise between maximum Ln^{3+} loading and selectivity was observed, driven by the variation in the quantity of weakly H-bonded TOPO and the change in the configurational entropy of the mixture. All results point towards the need to explicitly consider the HES phase structuration and its compositional changes with solute co-extraction on the Ln^{3+} extraction as no change in the extracted complex speciation was observed across all tested conditions. The $C_{10}OOH$+TOPO was used as a model system due as lanthanide extraction using TOPO and carboxylic extractants is well described whilst the phase diagram and properties of the eutectic are reported. Nevertheless, the derived

conclusions are translatable to other systems and can help guide the design and application of possible HES combinations for SX.

Keywords: Deep eutectic solvents; Type V eutectic; Solvent extraction; Hydrogen bonding; Small Angle X-ray Scattering

INTRODUCTION

Sustainable metallurgy stands uniquely poised to reduce the environmental impact of primary ore extraction whilst providing new avenues for the metallic value recovery from secondary "urban ores" including the rapidly growing electronic waste, thereby closing the loop.[1,2] Of the various metallurgical options, hydrometallurgy is hailed as the environmentally friendly alternative to the industrially preferred pyrometallurgical option due to its ability to recover metals from low-grade matrices, gentler process conditions and greater flexibility, solvent regeneration and limited gaseous emissions.[3] The hydrometallurgical process is divided in three major steps: leaching, separation and refining. Solvent extraction (SX) represents the major industrial mean to separate and purify many metal ions including copper, zinc, platinum group metals, uranium or lanthanides from complex leachates through their transfer from an aqueous to an immiscible organic phase.[4,5] This is typically achieved by means of amphiphilic molecules, named extractants, with a chelating polar group to ensure metal coordination and an apolar part stabilising the resulting complex in the organic phase. However, complex process flowsheet arising from the poor separation selectivity between similar elements results in the use of significant volumes of corrosive effluents and hazardous organic solvents and limits the wider applicability of SX.

For example, the stable oxidation state of +3 and near-identical chemistries of trivalent lanthanide cations (Ln^{3+}) renders their mutual separation both technologically and environmentally challenging.[6,7] The shielded nature of the 4*f* Ln valence electrons makes the interactions with ligands electrostatic (rather than covalent) in nature, with the coordination numbers and complex geometries determined mainly by steric factors.[8] In the absence of redox accessible pairs in aqueous media for most Ln^{3+}, SX separation relies on the small monotonic changes in the properties brought about by poor 4*f* electrons shielding and the gradual decrease of the ionic radius along the series from La^{3+} to Lu^{3+}, also known as the lanthanide contraction. The thermodynamic similarity of Ln^{3+} leads to small changes of less than 6.5 kJ mol^{-1} in binding affinities between adjacent cations.[9] The almost linear evolution of the stability constants, irrespective of the ligand nature,[9–12] attests to the difficulty in achieving a selective extraction of neighbouring pairs based on speciation alone. The fundamental chemistry problem behind Ln^{3+} separation is one of global importance. The mutual separation of Ln^{3+}, identified as one of the key separation challenges of the 21st century,[6] occurs over approximately dozens of counter-current extraction stages and is conservatively estimated to account for 30% of the total associated environmental impacts of Ln^{3+} oxide production.[5,13]

This generates substantial volumes of volatile and potentially toxic organic effluents due to relatively dilute operating conditions applied, from ppm levels to approximately 15 g L^{-1} of target solute.

In this context, the development of advanced functional solvents presenting increased efficacy with decreased environmental impacts is highly relevant. Hydrophobic eutectic solvents (HES) emerged as promising substitutes for the traditional apolar phase in SX.[14] HES are low-melting binary mixtures that present interesting properties due to the liquefaction and enhanced solubility provided by the decrease of the melting point of the mixture when compared to those of the starting pure constituents.[15] Extractant molecules can be incorporated as one of the two components of a eutectic systems, acting both as the apolar phase former and chelating agent thereby allowing for greater extractant concentrations and more intensive separation processes. This was successfully demonstrated for the extraction of uranyl, platinum group metals, transition metals, boron or lithium.[16–23] To the best of our knowledge, only one work systematically studied the partition of Ln^{3+} in a ternary HES of 1-decanol:oleic acid:bis(2-ethylhexyl) amine.[24] The suppressed Y^{3+} extraction resulted in an improved separation of the heavier Ln^{3+} whilst the loaded HES could be easily stripped reused over multiple SX cycles. Through judicious selection of the hydrophobic components, which can include cheap natural products such as terpenoids, fatty acids and/or alcohols,[15] HES avoid the use of organic diluents whilst presenting negligible water solubilities and viscosities associated with ionic solvents for SX. Furthermore, HES present the added advantage that no new compounds are synthesised, relying solely on the molar ratio of the components thereby simplifying the economical, toxicological, and environmental assessment.

First coined in 2003,[25] the prefix *deep* is assigned for eutectic mixtures for which the eutectic point temperature should be lower to that of an ideal liquid mixture.[15] The increased melting point depression stems from the stronger intermolecular interactions between the eutectic components relative to those present in the pure compounds.[14,26] Relating this "deepness" to SX, there is growing evidence that metal extraction in strongly non-ideal HES[27,28] proceeds differently to that in ideal or quasi-ideal systems.[29] The free energy of transfer for a given electrolyte in SX can be decomposed into three main contributions, namely (i) the favourable complexation energy of the metal ion and extractant, which is partially quenched by (ii) solute confinement in the highly concentrated polar domains of the organise phase and (iii) solvent-phase nano-structure reorganization around the extracted and coextracted species ($\Delta G_{Structuration}$).[30,31] Compared to conventional SX in which the organic phase structuration is

often a consequence of metal ions and polar solute extraction,[32] mixed extractant interactions[33,34] as well as diluent effects[35] are expected to be more important when using HES due to the intrinsic nature of the solvent. HES presenting negative thermodynamic deviations from ideality yield highly structured liquid phase defined by intermolecular interactions.[36] These solvents are characterised by hydrogen bonding (H-bonding) to yield sterically crowded pre-organised phases, the nature of the latter depending on the selection of the hydrogen bond donor (HBD) and acceptor (HBA) components and their respective molar ratio. The organisation of DES translates into the presence of structural heterogeneity and the formation of defined polar domains as shown for the thymol + menthol system by small-angle X-ray scattering analysis (SAXS).[36]

Pre-organisation of the solvent phase is in some cases viewed as undesirable due to the potential for an antagonistic extraction mechanism.[37] Comparatively, less attention has been paid to the possibility of tuning the selectivity by controlling the dynamics and mesoscale organisation of a "concentrated" SX organic phase.[32,38] The control of the intermolecular interactions dictating the hierarchical self-assemblies in SX, and therefore the magnitude of the $\Delta G_{Structuration}$ contribution, affords a new avenue for the design of next-generation separation techniques. As structured solvent phases in SX are in dynamic equilibrium, considering only the first solvation sphere of the extracted ions provides a limited assessment of the SX free-energy landscape and does not fully exploit the potential stabilising forces over longer correlation lengths, such as second neighbour and percolation effects. H-bonding in the "soft" outer-sphere of "hard" metal-ligand complexes with non-ionic extractants plays a critical role in determining the selectivity of lanthanide separation.[39,40] Additionally, the abundant presence of H-bonds in the apolar phase of SX was shown to swell the polar network volume, yielding an increase in the extraction efficiency of metal ions that are solubilised but non-chelated (i.e. no modification of the actual metal-ligand complexation energy).[41–43] Finally, H-bond donors are commonly added as phase modifiers to prevent the critical phenomenon of third-phase formation in which the apolar phase splits into a heavy and light phase upon extraction of polar solutes above a certain concentration.[44] An analysis of these effects upon metal extraction in HES merits further investigation and could be of interest for difficult separation that typically rely on small variations of complexation energies.

In this work, the SX of selected light, middle and heavy lanthanides from nitric acid media is studied in the H-bonded assembly that is the deep HES of trioctylphosphine oxide (TOPO) and decanoic acid ($C_{10}OOH$). The choice of potential HES combinations is restricted by the

chemical stability of the hydrogen bond donor in the presence of the strongly oxidising HNO_3 acid, such that most phenolic and alcohol compounds are excluded. The TOPO+C_{10}OOH phase diagram was previously reported and shows strong negative deviations to ideality manifested by a melting point depression of 29.2 K below that predicted for an ideal system and a large liquidus composition (at 298 K) spanning a TOPO molar fraction (x_{TOPO}) range of 0.10 to 0.55.[18] Furthermore, lanthanide extraction using TOPO and the equivalent Cyanex 923 is well described,[45–47] facilitating the comparison between SX in the studied HES and conventional diluents. Through the systematic variation of metal cation type, x_{TOPO}, and HNO_3 concentration, the delicate balance between complexation and solvent reorganisation and its influence on the extraction and metal selectivity is determined. The obtained trends can expand and guide the design and application of possible HES combinations based on well-known non-ionic lanthanide ligands such as phosphate, diglycolamide or malonamide-type extractants.

METHODOLOGY

Reagents

Trioctylphosphonine oxide (TOPO) (99%), thymol (99-101%), decanoic acid (99%) (C_{10}OOH), nickel nitrate hexahydrate (>98.5%), neodymium nitrate hexahydrate (99.9%), praseodymium nitrate hexahydrate (99.99%), yttrium nitrate hexahydrate (99%), lanthanum nitrate hexahydrate (99.99%), and cerium (III) nitrate hexahydrate (99.99%) were obtained from Sigma Aldrich (USA). Iron chloride (III) hexahydrate (98%), sodium nitrate (99%), and nitric acid 65% were obtained from Vetec (Brazil). Solutions of Ce^{4+} (9.585 mg g^{-1}), Eu^{3+} (9.577 mg g^{-1}), Gd^{3+} (9.683 mg g^{-1}) and Lu^{3+} (9.683 mg g^{-1}) were obtained from Specsol (Brazil). Trioctylamine (TOA, 98%) was obtained from Fluka (USA).

Solute Partition

The partition of metal ions [La^{3+}, Ce^{3+}, Ce^{4+}, Pr^{3+}, Nd^{3+}, Eu^{3+}, Gd^{3+}, Y^{3+}, and Lu^{3+}] was performed in a two-phase liquid system formed by the mixture of 0.50 g of HES C_{10}OOH + TOPO (molar fraction of TOPO of either 0.3, 0.4 or 0.5) with 1.0 g aqueous solution of HNO_3 (from 0.10 to 6.0 mol L^{-1}) or 2.0 mol L^{-1} of $NaNO_3$. A constant individual metal ion concentration of 7.5 mmol kg^{-1} was used throughout. Additionally, the partition of Eu^{3+} and Lu^{3+} was studied as a function of temperature from 293 to 343 K for two HNO_3 concentrations (1.0 and 6.0 mol L^{-1}) and three x_{TOPO} (0.3 to 0.5). The mixture of HES and aqueous solution

was always performed under agitation of 1 min and the separation of phases accelerated by centrifugation at 10000 rpm for 5 min. The metal content in the aqueous phase before and after extraction was analyzed via Microwave Plasma Atomic Emission Spectroscopy (MP-AES, Agilent Technologies, USA). The partition of HNO_3 under the same extraction conditions in the absence of metal cations was determined by UV-Vis analysis of the aqueous phase (Shimadzu, UV-2550, TCC-240, Japan) through the absorbance peak at 301 nm (calibration curve determined from 0.1 to 0.8 mol L^{-1}) using a quartz cell with a path length of 1 cm. The water content in the HES phase following extraction was measured using a coulometric Karl Fischer titrator (Metrohm 831, Switzerland) with an Hydranal® solution from Sigma-Aldrich. Due to the incompatibility of the HNO_3 with the titrating solution, the organic phase was first neutralised using TOA prior to titration following a reported methodology as the resulting [TOAH][NO_3] is soluble in the HES.[48] An excess of TOA (0.1 g) was added to 0.5 g of the HES sample and agitated at 298 K for 1 h prior to measurement. The water content of the sample was corrected considering the water content of pure TOA that was independently measured.

Luminescence Measurements

The emission and excitation spectra were recorded at ambient-temperature using a Fluorolog®-3Horiba Scientific (Model FL3-2T) spectroscope. with a modular double grating excitation spectrometer (fitted with a 1200 grooves/mm grating blazed at 330 nm) and a TRIAX 320 single emission monochromator (fitted with a 1200 grooves/mm grating blazed at 500 nm. reciprocal linear density of 2.6 $nm.mm^{-1}$) coupled to a R928 Hamamatsu photomultiplier. using the front face acquisition mode. The excitation source was a 450 W Xe arc lamp. The emission spectra were corrected for detection and optical spectral response of the spectrofluorimeter and the excitation spectra were corrected for the spectral distribution of the lamp intensity using a photodiode reference detector. Time-resolved measurements have been carried out using a 1934D3 phosphorimeter coupled to the Fluorolog®-3. and a Xe-Hg flash lamp (6 μs/pulse half width and 20-30 μs tail) was used as the excitation source.

Raman spectroscopy

Raman spectra were acquired on a Bruker MultiRAM equipped with a 1064 nm Nd-YAG laser source and a nitrogen cooled germanium detector. All spectra were recorded in the 3600 to 100 cm^{-1} range with a resolution of 4 cm^{-1}. A total of 500 scans and a laser power of 350 mW and was applied. The obtained spectra were deconvoluted using the Origin software package. The

baseline was fitted using an exponential decay function and subtracted. The resulting area was deconvoluted into Lorentzian components.

Small-Angle X-ray Scattering (SAXS) Measurements

SAXS experiments were performed using a home-built SAXS camera at the Institut de Chimie Séparative de Marcoule (ICSM). The setup involves a molybdenum source delivering a 1 mm circular beam of energy at 17.4 keV. A monochromatic beam was obtained by using a Fox-2D multishell mirror, and collimation of the beam was achieved using 2 sets of "scatterless" slits, which are crucial for the quantification of weak scattering near the beam-stop, together with precise monitoring of the transmission of the sample and solvents used as the reference. The scattering pattern was recorded using a MAR345 two-dimensional imaging plate, with a typical duration of 1 h. The measurements were performed in transmission geometry using 2 mm glass capillaries. The experimental resolution was set to $\Delta q/q$ = 0.05. The detector count was normalised to the differential cross-section per unit volume (in cm^{-1}) with either a 2.36 mm thick high-density polyethylene sample (from Goodfellow®) (I_{max} = 5.9 cm^{-1}) or 3 mm water for which the level of scattering at low q is known (1.64 × 10^{-2} cm^{-1}). Data pre-analysis was performed using PYSAXS software, considering the electronic background of the detector (where the flat-field response was homogeneous), transmission measurements (using a photodiode that can be inserted upstream of the sample), and empty cell subtraction. The scattering intensities are expressed as a function of the magnitude of the scattering vector.

RESULTS AND DISCUSSION

SX in TOPO+C_{10}OOH – general considerations

In SX, the extraction strength for a given lanthanide ion (Ln^{n+}) is expressed as the distribution ratio (D_{Ln}) shown in equation (1) whilst the selectivity reflects the affinity of the system for one Ln^{n+} cation over another and is expressed by the separation factor (SF) in equation (2).

$$D_{Ln} = \frac{[Ln]_{HES}}{[Ln]_{aq}} \quad \text{- (1)}$$

$$SF_{Ln1/Ln2} = \frac{D_{Ln1}}{D_{Ln2}} \quad \text{- (2)}$$

where "HES" and "aq" indicate the concentration of Ln in the HES and aqueous phase respectively. In non-ionic systems, D_{Ln} and SF depend not only on the capacity of the organic

phase to accommodate the ionic lanthanide species but also the nature and concentration of the accompanying counter-ions to ensure charge neutrality. The extraction mechanism for Ln^{3+} using 0.2 mol L^{-1} TOPO diluted in toluene (not considering water molecules) was previously determined based on slope analysis as:[46,49]

$$Ln_{aq}^{3+} + 3NO_{3,aq}^{-} + 3TOPO_{org} \leftrightarrow [Ln(NO_3)_3(TOPO)_3]_{org} \quad \text{- (3)}$$

Whilst slope analysis regression is possible for systems that can be described using a simple set of equilibria, this approach does not properly describe complex extraction mechanisms with multiple equilibria as can occur in the case of mixtures such as HES.[30] In the latter, as TOPO is both the chelating agent and one of the eutectic phase former, the ratio between the concentration of free extractants for SX and the total concentration in the system is blurred. An additional consideration is the role of $C_{10}OOH$ on the distribution as carboxylic acid-based extractants such as Versatic 10 are known as lanthanide extractants.[50] Throughout this work, the systematic variation of the HES phase composition is represented by the change in the TOPO molar fraction x_{TOPO}. However, as $x_{TOPO} = 1 - x_{C10OOH}$ in the HES phase, such variations in composition also address the role of $C_{10}OOH$ on the extraction and liquid phase organisation. To simplify the system interpretation, reduce emulsification and loss of the HES component to the aqueous phase, extraction was investigated for aqueous phase acidities below the pKa (~4.9) of $C_{10}OOH$. Under such conditions, carboxylic-based extractants are not reported to extract lanthanide.[50] Nevertheless, $C_{10}OOH$ can interact with TOPO as well as stabilise co-extracted nitrate anions and molecular nitric acid thereby indirectly contributing to Ln^{3+} extraction. Considering these limitations, no effort was made to rationalise the obtained D_{Ln} through slope analysis. Rather, D_{Ln} values were used to determine the Gibbs free energy of transfer of a metal ion (ΔG_R) given by equation (4) as there is no assumption of a dominant supramolecular extraction equilibrium that would consider all other species present in the solution.[51]

$$\Delta G_R = -RTln(D_{Ln}) \quad \text{- (4)}$$

In equation (4), the reaction Gibbs energy of the transfer standard state is defined for a solvent containing all the species but lanthanide salt. It is therefore the free energy per mole of the transferred species and not the raw difference of a given sample versus a reference state, as classically noted ΔG^0 in thermodynamics.

SX in TOPO+C_{10}OOH – influence of HNO_3 concentration

In a first instance, the influence of the aqueous HNO_3 concentration from 0.1 to 6.0 mol L^{-1} on the extraction of La^{3+}, Ce^{3+}, Pr^{3+}, Nd^{3+}, Eu^{3+}, Gd^{3+}, Y^{3+} and Lu^{3+} by the C_{10}OOH+TOPO HES was determined and presented in **Figure 1A**. Y^{3+} was used as a proxy for Ho^{3+} due to their similar ionic radii and are discussed interchangeably in the rest of this work. A constant metal concentration of 7.5 mmol L^{-1}, organic to aqueous phase ratio (O/A) of 0.5, T = 298 K, and TOPO molar fraction of 0.5 were applied. All reported D_{Ln} values are available in **Table S1-S4** of the ESI. It is important to note that (i) no third-phase formation was observed and (ii) no loss of the HES component to the aqueous phase after extraction was detected by ^{1}H-NMR (detection limit of 5 mol.%) for any of the extractions performed.

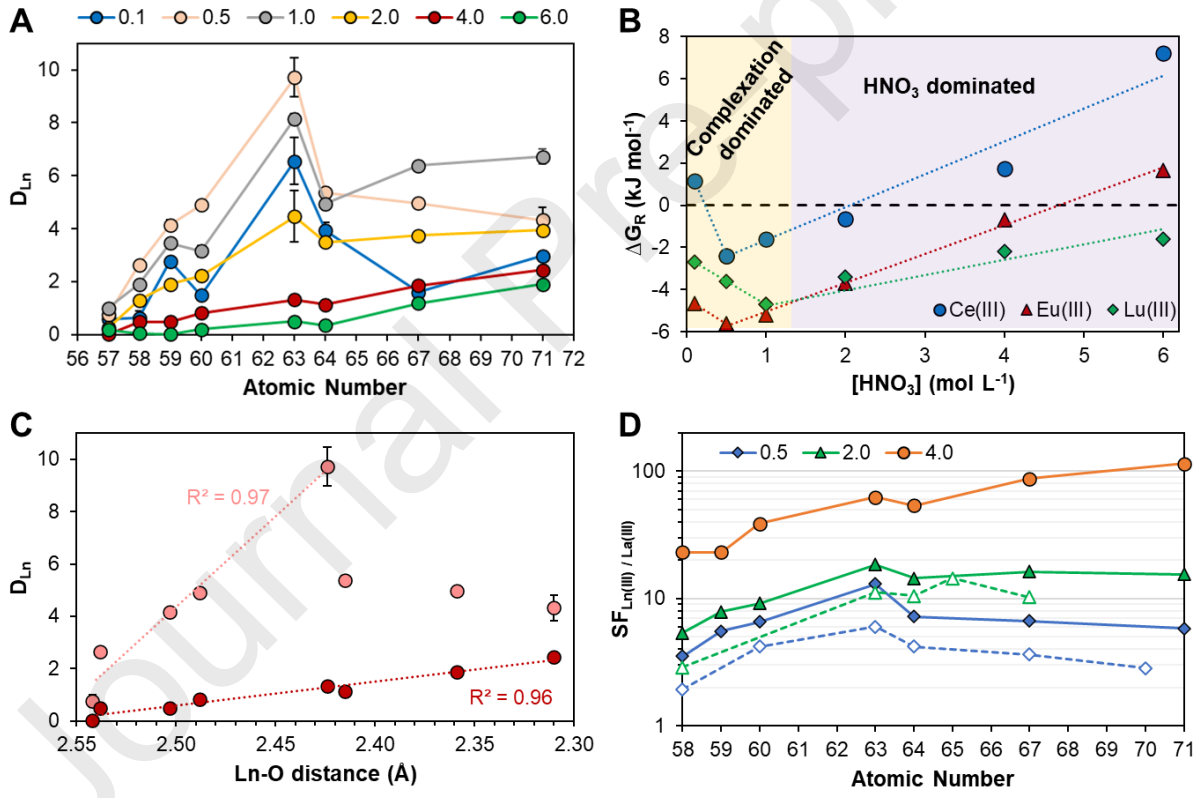

Figure 1. A) Distribution coefficients (D_{Ln}) and B) Gibbs free energies of transfer of Ln^{3+} in the C_{10}OOH+TOPO HES as a function of the initial aqueous phase HNO_3 concentration (O/A = 0.5, x_{TOPO} = 0.5, [Ln^{3+}] = 7.5 mmol L^{-1}). C) D_{Ln} as a function of the ionic radii of trivalent lanthanide cations (taken from ref [52]) for two HNO_3 concentration of 0.5 and 4.0 mol L^{-1}. D) Separation factors for Ln^{3+}/La^{3+} pairs in the C_{10}OOH+TOPO HES for a fixed HNO_3 concentration of 0.5, 2.0 and 4.0 mol L^{-1} (full lines) and compared against traditional SX using

TOPO at the same HNO_3 concentration (dashed lines) taken from refs [46,47]. Lines are drawn to help the eye. In all cases Y^{3+} is used as a proxy for Ho^{3+}.

As shown in **Figure 1A**, the distribution ratios irrespective of the lanthanide ion present a maximum for $0.5 \leq [HNO_3] \leq 1.0$ mol L^{-1} and decrease thereafter with increasing $[HNO_3]$. The speciation of trivalent lanthanides for the studied HNO_3 range does not significantly vary, with the $[Ln(H_2O)_n]^{3+}$ (n=8 or 9) and $[Ln(NO_3)(H_2O)_{n-1}]^{2+}$ reported to be the dominant aqueous phase complexes at the lowest and highest HNO_3 concentration investigated respectively.[53,54] By ruling out the influence of speciation, the decrease of D_{Ln} is attributed to the competitive co-extraction of HNO_3 (*infra vide*).[55–57] HNO_3 is a fairly weak inorganic acid and its protonated and dissociated form exist in equilibrium above 3.0 mol L^{-1},[58] with the equilibrium shifted towards the protonated specie in lower-dielectric media.[59] Plotting ΔG_R as a function of the initial aqueous HNO_3 concentration for one light, middle and heavy lanthanide (**Figure 1B**) clearly identifies two extraction regimes in which ΔG_R varies monotonically. The first regime is dominated by Ln^{3+}•TOPO complexation for $[HNO_3] \leq 1.0$ mol L^{-1} whilst the second is influenced by the HES phase re-organization induced by acid co-extraction for $[HNO_3] \geq 1.0$ mol L^{-1} as will be demonstrated further on. No inferences are made as to the extraction mechanism and stoichiometry of the metal-extractant chelate in these two regimes and if these differ at all.

The shift between extraction regimes not only changes the distribution ratio for a given lanthanide but also varies the D_{Ln} trend along the Ln series. This is exemplified in **Figure 1C** by plotting the D_{Ln} obtained for a fixed HNO_3 concentration of 0.5 and 4.0 mol L^{-1} against the ionic radii of trivalent Ln^{3+} cations.[52] At lower HNO_3 concentrations, the D_{Ln} suggest a tetrad effect[60] and present two clear groupings. An initial rise in D_{Ln} is observed with the increasing charge density of the Ln cation, reaching a maximum for Eu^{3+}, followed by a sharp decrease from Eu^{3+} to Gd^{3+} and further reductions in D_{Ln} for heavier Ln. A similar maximum D_{Ln} range from Eu^{3+} to Tb^{3+} (depending on the study) was observed for TOPO in conventional organic diluents for a HNO_3 concentration of 0.5 mol L^{-1}.[46,47] A notable difference upon inclusion of TOPO in HES is the sharp break in D_{Ln} between the adjacent Eu^{3+} and Gd^{3+}, which was not observed in the conventional SX, yielding an interesting $SF_{Eu/Gd}$ of 1.81 at this acid concentration. Although no clear "gadolinium break" was observed in the coordination number of hydrated lanthanides,[61] Gd^{3+} is often considered as a transition point between the nine-

coordinate structure preferred by the lighter lanthanides and the eight-coordinate structure of the heavier Ln.[61,62] The break in D_{Ln} with decreasing ionic radius after Eu^{3+} is therefore assigned to steric hindrances to coordination by bulky TOPO ligands imposed by the change in Ln^{3+} coordination number and further exacerbated by the sterically crowded nature of the HES phase. This is consistent with the variation in the coordination number of Ln^{3+} nitrate complexes with triethylphosphine oxides (Et_3PO) from $Ln(NO_3)_3(Et_3PO)_3$ for the lighter lanthanides to mixtures of $Ln(NO_3)_3(Et_3PO)_3$ and $Ln(NO_3)_3(Et_3PO)_2$ for the heavier metals as determined from single crystal X-ray crystallography.[49,63] In fact, the apparent equilibrium constant for Ln^{3+} extraction from nitrate media using phosphine oxide extractants presenting a lesser steric restriction is found to increase with decreasing ionic radii as shown in **Figure S1** and in contrast to the results in **Figure 1A**, further confirming the influence of the complex geometry on the measured D_{Ln}.

Raising the initial aqueous HNO_3 concentration to 4.0 mol L^{-1} suppresses the extraction of the lighter Ln^{3+} relative to the heavier ones and eliminates the break in D_{Ln} at Eu^{3+}, resulting in the linear increase of D_{Ln} with decreasing ionic radius as shown in **Figure 1C**. The change in extraction regime from an "complexation dominated" one to "HNO_3 dominated" is reflected in the D_{Ln} trends, as shown in **Figure 1B-C**, and by extension in the derived separations factors. The SFs between Ln^{3+} and La^{3+} as reference for three initial HNO_3 concentrations of 0.5, 2.0 and 4.0 mol L^{-1} are presented in **Figure 1D** and compared, when available, with reported SX data for TOPO in organic diluents at the same acid concentration.[46,47] Similar trends in the $SF(Ln^{3+}/La^{3+})$ between SX in HES and in conventional system for 0.5 and 2.0 mol L^{-1} HNO_3 are obtained albeit with increased SFs in HES due to the consistently poor partition of La^{3+} across all tested acid concentrations. This confirms that non-ionic extractants can be incorporated as HES constituents without losing their extraction characteristics. Under mildly acidic conditions, a maximal SF is obtained for the Eu/La pair in HES media with $SF_{Eu/La}$ = 13.0 and 18.4 for 0.5 and 2.0 mol L^{-1} HNO_3 respectively. However, for $[HNO_3] \geq 4.0$ mol L^{-1} a change in the selectivity is observed, permitting the efficient separation of heavy from light Ln^{3+} with a $SF_{Lu/La}$ = 114.7 at 4.0 mol L^{-1} HNO_3. The observed tendencies are similar to that for tributyl phosphate (TBP) extractant in which a maximum extraction is obtained for Gd^{3+} at HNO_3 concentrations below 4.0 mol L^{-1} ($SF_{Eu/La}$ ~20) but D_{Ln} proceeds in an approximately linear manner from light to heavy Ln^{3+} at HNO_3 concentrations above 10.0 mol L^{-1} ($SF_{Lu/La}$ ~100).[64,65] The obtained $SF_{Lu/La}$ is comparable to other conventional SX systems using solvating extractants such as Cyanex 923 ($SF_{Lu/La}$ = 200 at $[NaNO_3]$ = 1.0 mol L^{-1} and pH =

3)[66] or *N*,*N*,*N*′,*N*′-tetraoctyl diglycolamide (TODGA; $SF_{Lu/La}$ = 119 at [HNO_3] = 1.0 mol L^{-1})[67] albeit achieved in HES at much higher acid concentrations. Finally, Ln^{3+} extraction in nitrate media by TOPO dissolved in "inert" alternative solvents such as non-functionalised fluorinated ionic liquids present improved by variable D_{Ln} and resulting SFs values between heavy (Yb^{3+}) and light (La^{3+}) Ln^{3+} from 185 to over 5000. This difference is attributed to the nature of the ionic liquid cation and the extent of its cation-exchange with Ln^{3+}, implying a partial loss of the IL constituents to the aqueous phase with use. Furthermore, extraction was supressed for pH values below 1, limiting its applicability under acidic conditions.[68]

The possibility to alter the D_{Ln} trend in HES by acid co-extraction allows the manipulation of weak interactions (i.e. non-electrostatic) to tune the SFs and achieve a compromise between maximising extraction and enhancing separation for a target lanthanide. To highlight this, substitution of HNO_3 by 2.0 mol L^{-1} $NaNO_3$, a stronger salting-out agent that is poorly extracted due to its less favourable Gibbs free energy of hydration, enhances the complexation of the Ln^{3+} cations with TOPO. Being not extracted, it is not expected to provoke any restructuration of the HES phase. When using $NaNO_3$, close to quantitative extraction of all Ln^{3+} was obtained as shown in **Figure 2**, resulting in D_{Ln} >> 100 for all cations but a decrease in the overall selectivity of the system.

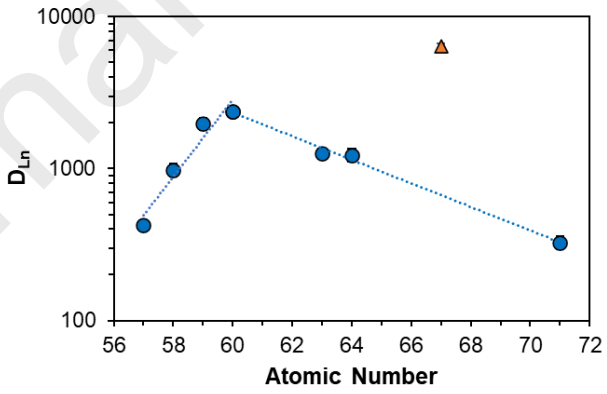

Figure 2. Distribution coefficients of Ln^{3+} in the C_{10}OOH+TOPO HES for an initial aqueous phase concentration [$NaNO_3$] = 2.0 mol L^{-1} (O/A = 0.5, x_{TOPO} = 0.5, [Ln^{3+}] = 7.5 mmol L^{-1}). Lines are drawn to help the eye.Y^{3+} is indicated by the orange triangle. D_{Ln} values are available in **Table S2**.

SX in TOPO+C_{10}OOH – influence of TOPO molar fraction

Beyond the aqueous phase acid concentration, another approach to manipulate the HES phase pre-organization is through the variation of the HBD to HBA ratio. Whilst the liquid structure of HES is dynamic in nature, the change in the C_{10}OOH to TOPO ratio is expected to vary the energy landscape for the various possible interspecies interactions between the HES constituents and extractable polar species.[27] As such, the influence of HES phase structuration is further investigated through the change in TOPO molar fraction from x_{TOPO} = 0.3 to 0.5 at two HNO_3 concentrations of 1.0 and 6.0 mol L^{-1} for one light (La^{3+}), middle (Eu^{3+}) and heavy lanthanide (Lu^{3+}). A constant metal concentration of 7.5 mmol L^{-1}, O/A = 0.5 and T = 298 K were applied. In addition, the influence of the Ln oxidation state was monitored by following the extraction of Ce^{4+} under the same conditions. The obtained distribution factors are shown in **Figure 3A-B** and available in **Table S3** of the ESI.

A reduction in the x_{TOPO} yields a decrease in all D_{Ln} although the extent of the relative decrease from x_{TOPO} of 0.5 to 0.3 varies with the HNO_3 concentration as well as the nature of the Ln and its oxidation state. At 1.0 mol L^{-1} HNO_3 (**Figure 3A**), extraction of La^{3+} is suppressed allowing, for example, to raise the $SF_{Lu/La}$ from 6.7 to 16.0 as x_{TOPO} decreases from 0.5 to 0.4 respectively despite the lower D_{Lu} values. No extraction of trivalent lanthanides was observed for x_{TOPO} = 0.3. A similar tendency of D_{Ln} with x_{TOPO} is observed at 6.0 mol L^{-1} HNO_3 (**Figure 3B)** for the lighter and middle lanthanides. In contrast, D_{Lu} remains comparatively unaffected, yielding in an improved selectivity of the difficult Lu/Eu pair separation from 3.7 to 24.9 as x_{TOPO} changes from 0.5 to 0.3 respectively. Contrary to conventional SX in which the distribution of Ln^{3+} cations varies predictably with the extractant concentration as shown in equation (3),[46,49] the same was not observed in HES. To highlight this, the logarithm of D_{Ln} presented in **Figure 3A-B** were plotted against that of the TOPO concentration in the HES, with the resulting graphical slope analysis presented in **Figure S2**. Sterically impossible slope values of 16.7 and 9.9 were obtained for Eu^{3+} and Lu^{3+} respectively at 1.0 mol L^{-1} HNO_3 with these values decreasing to 2.3 and 7.9 at 6.0 mol L^{-1} HNO_3. Such unrealistic values and their change with the aqueous phase acidity emphasises both the difference in the two extraction regimes and the inability of slope analysis to adequately capture the extraction mechanism in these complex systems.

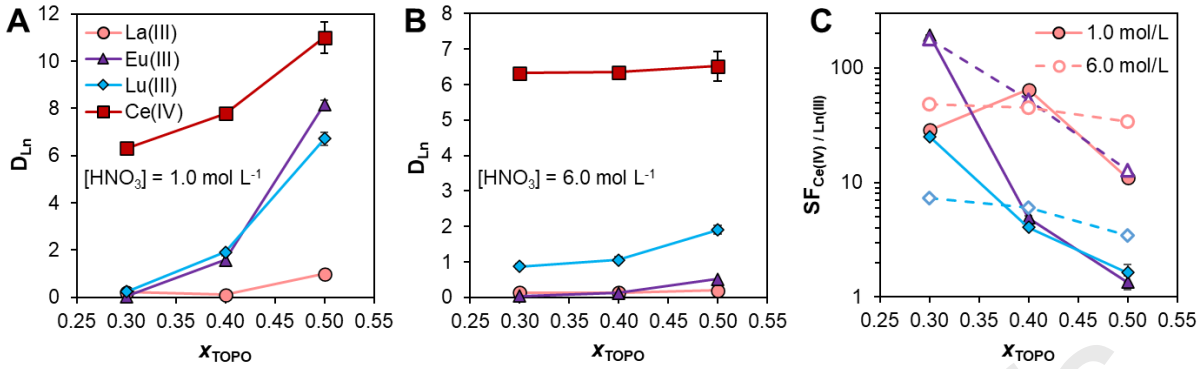

Figure 3. Lanthanide distribution coefficients in the $C_{10}OOH$+TOPO HES as function of the x_{TOPO} molar fraction for two initial aqueous phase HNO_3 concentrations of A) 1.0 and B) 6.0 mol L^{-1}. C) Derived Ce^{4+}/Ln^{3+} separation factors (O/A = 0.5, [Ln] = 7.5 mmol L^{-1}).

Unlike the trivalent Ln^{3+}, tetravalent cerium is efficiently extracted across all tested compositions. Ce^{4+} is often used as a relevant but non-radioactive analogue of tetravalent actinides, especially of Np^{4+} and Pu^{4+},[69] which could be of interest towards the PUREX process when also considering the reported affinity of TOPO-based DES for uranyl nitrate.[20] Comparison of the distribution ratio of Ce^{3+} and Ce^{4+} with HNO_3 concentration for x_{TOPO} = 0.5 is presented in **Figure S3** and shows a maximum separation of the tetravalent from trivalent state at 6.0M HNO_3 with $SF_{Ce(IV)/Ce(III)}$ = 119.4. At this acid concentration, Ce^{4+} extraction is independent of the HES phase TOPO concentration as shown in **Figure 3B** and **Figure S2**. The selectivity towards the higher valency Ce^{4+} is consistent with the greater charge density of the cation as well as possible speciation effects at higher HNO_3 concentrations at which polynuclear oxo-bridged Ce^{4+} complexes of the type $[(H_2O)_6Ce_2O(NO_3)_6]$ were reported.[69,70] Modification of x_{TOPO} can be further harnessed to improve the Ce^{4+} selectivity towards middle and heavy lanthanides at the investigated HNO_3 concentration as shown in **Figure 3C**. By exploiting the inefficient extraction of the trivalent lanthanides at lower x_{TOPO} compositions, an improved Ce^{4+}/Eu^{3+} and Ce^{4+}/Lu^{3+} separation factors of 195.1 and 25.3 respectively were achieved at 1.0 mol L^{-1} HNO_3 and x_{TOPO} = 0.3 compared to the corresponding negligeable values of 1.34 and 1.64 obtained for x_{TOPO} = 0.5. Interestingly, results in **Figure 3A-B** show that the extraction dependency of Ln^{3+} and Ce^{4+} with the initial aqueous HNO_3 concentration is reduced for lower x_{TOPO}, this being consistent with the negligible HNO_3 extraction and restructuration effects for x_{TOPO} = 0.3 discuss further on.

An important assumption made so far in the rationalisation of D_{Ln} trends with HNO_3 concentration and initial HES composition, namely on the importance of the HES pre-organisation on the extraction, is the unvaried nature of the extracted metal complex in the HES phase. As such, the mechanism of extraction in the $C_{10}OOH$ + TOPO HES at three TOPO molar fraction is studied using two complementary approaches aiming to detangle the respective contribution of complexation and HES phase structuration on the D_{Ln}. First, a time resolved fluorescence spectroscopy (TRFS) using Eu^{3+} as probe is carried out to determine the nature of inner sphere of the metal-solvate species. Second, the HES phase organisation after equilibration with aqueous phases of differing acidity was followed by Raman spectroscopy and small-angle X-ray scattering (SAXS). A fixed condition of O/A = 0.5 and T = 298 K was applied throughout.

SX in TOPO+C_{10}OOH – influence of speciation

The fine structure and the relative intensities (asymmetry ratio values) of the transitions in the excitation and emission spectra of Eu^{3+} reflects the local point group symmetry of the Eu^{3+}-ligand complex whilst the number of water molecules present in the primary coordination sphere of Eu^{3+} can be gleamed from the decay profile and lifetime of its transition.[71,72] To ensure that measurable intensities were obtained for all HES phase compositions (x_{TOPO} from 0.3 to 0.5), the Eu^{3+} aqueous phase concentration was increased to 0.1 mol L^{-1} and the extraction was performed in 1.0 mol L^{-1} HNO_3 supplemented with 0.5 mol L^{-1} $NaNO_3$ as salting-out agent. The obtained D_{Eu} as well as the final HES-phase water content measured by Karl-Fisher titration for each x_{TOPO} are reported in **Table 1**. The resulting normalised excitation spectra (emission at 616.5 nm) and emission spectra (excitation at 394.0 nm) with the identified transitions[71] are presented in **Figure 4A-B** whilst the TRFS of the Eu^{3+} $^5D_0 \rightarrow {}^7F_2$ transition after excitation at $^7F_0 \rightarrow {}^5L_6$ .is shown in **Figure 4C**.

Table 1. D_{Eu} and HES-phase water content after extraction of Eu^{3+} ($[Eu]_{aq,ini}$ = 0.1 mol L^{-1}) from an aqueous solution containing 1.0 mol L^{-1} HNO_3 and 0.5 mol L^{-1} $NaNO_3$ for three x_{TOPO}. Resulting asymmetry ratio (AR, the ratio of $I_{616.5}/I_{591.0}$), luminescence lifetime (τ) and number of inner-sphere water molecules (n_{H2O}) of the extracted Eu^{3+} complex in the HES-phase.

x_{TOPO}	$[HNO_3]_{aq}$ (mol L^{-1})	D_{Eu}	$[H_2O]_{DES}$ (wt %)	AR	τ_{H2O} (ms)	τ_{D2O} (ms)	n_{H2O}
0.3	1.0	0.28 ± 0.09	1.49 ± 0.24	5.3	1.336	1.745	0.2
0.4	1.0	3.53 ± 0.23	1.33 ± 0.19	5.4	1.510	1.785	0.1
0.5	1.0	99.9 ± 3.69	1.26 ± 0.23	5.2	1.607	1.799	0.1
0.5	6.0	0.45 ± 0.03	0.98 ± 0.16	5.9	1.328	-	-

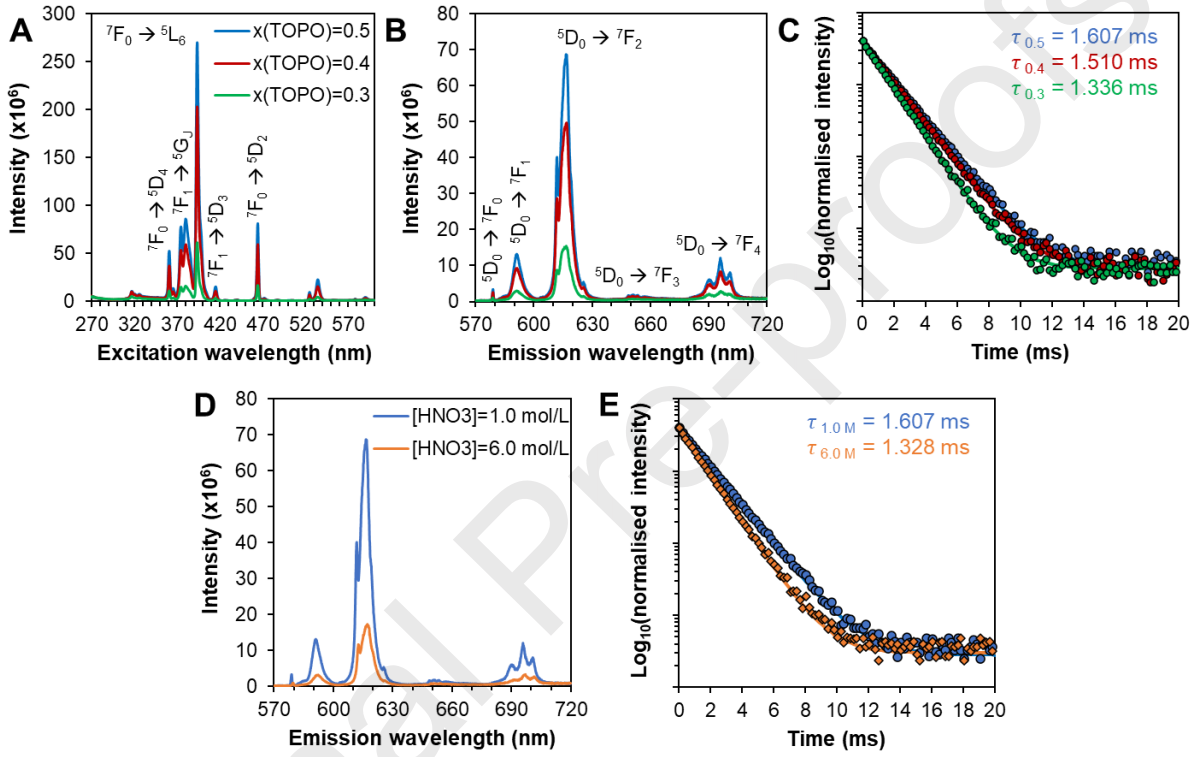

Figure 4. Normalised A) excitation spectra (emission at 616.5 nm), B,D) emission spectra (excitation at 394.0 nm), and C,E) time resolved fluorescence spectroscopy of the $^5D_0 \rightarrow {}^7F_2$ transition of Eu^{3+} after excitation at 394.0 nm as a function of x_{TOPO} (0.3 to 0.5) and aqueous phase HNO_3 concentration (1.0 or 6.0 mol L^{-1}) in the $C_{10}OOH$ + TOPO HES. Lines (overlapping data points) correspond to the single exponential decay fit. Description of the HES phase composition is provided in **Table 1**.

The observed transitions in the absorption spectra are due to the Laporte-forbidden f–f electronic transitions of Eu^{3+}. Of interest is the increased relative intensity and red-shifting of the hypersensitive $^7F_0 \rightarrow {}^5D_2$ transition in the HES phase relative to its aqueous spectrum, shown in **Figure S4**, suggesting the partial displacement of water molcules from the first

coordination sphere of Eu^{3+}. The luminescence spectra of Eu^{3+} in the $C_{10}OOH$ + TOPO for all molar fractions are defined by the $^5D_0 \rightarrow {}^7F_J$ (J = 0, 1, 2, 3, 4) transitions. The spectra are dominated by the hypersensitive $^5D_0 \rightarrow {}^7F_2$ transition, with an intensity approximately 5.3 times that of the $^5D_0 \rightarrow {}^7F_1$ transition (see **Table 1**), indicative of a geometry without an inversion center.[71] Additionally, a narrow band is observable for the $^5D_0 \rightarrow {}^7F_0$ transition characteristic of complexes with C_n, C_{nv} and C_s symmetry.[71] Of the possible coordination geometries, the only ones that allow a $^5D_0 \rightarrow {}^7F_0$ transition are the bicapped trigonal prism (coordination number = 8, C_{2v} symmetry) and the capped square antiprism (coordination number = 9, C_{4v} symmetry). The number of peaks in the $^7F_0 \rightarrow {}^5D_0$ excitation spectrum was also previously shown to correspond to the number of distinct local environments of the Eu^{3+} cation.[73] The existence of a sole $^5D_0 \rightarrow {}^7F_0$ transition for all compositions suggests that only one dominant Eu^{3+}-complex, most likely with a capped square antiprism geometry when considering the extraction results from **Figure 1**, is present in the HES phase. The TRFS data for all three HES compositions in H_2O is presented in **Figure 4C** whilst the same analysis in deuterated water (D_2O) is available in **Figure S5**. The decay profiles were fitted with a single exponential decay function from 0.0 to 6.0 ms and the lifetime (τ) of the $^5D_0 \rightarrow {}^7F_2$ transition are summarised in **Table 1** as well as the derived number of inner-sphere water molecules (n_{H2O}) obtained using equation (5).[72]

$$n_{H2O} = 1.05 \times \left(\frac{1}{\tau_{H2O}} - \frac{1}{\tau_{D2O}}\right) \quad \text{- (5)}$$

Considering the uncertainty associated with the n_{H2O} correlation of ±0.5 water molecules, it appears that the first coordination shell of Eu^{3+} is dehydrated for all HES phase composition and that the co-extracted water content in **Table 1** does not influence the nature of the metal ion complex. The decrease in the luminescence lifetime in H_2O as x_{TOPO} is reduced from 0.5 to 0.3 (**Figure 4C**) is therefore probably due to the presence of quenching species such as water or carboxylic acid molecules in the outer-sphere of the Eu^{3+} complex. Overall, luminescence measurements confirm that Eu^{3+} is present in the same chemical environment for all HES compositions.

SX in TOPO+C_{10}OOH – influence of HES-phase composition and structure

Having ruled out speciation (for a given Ln^{3+}) as a justification for the observed D_{Ln} trends in **Figure 1** and **3**, attention is now paid to the influence of the HES phase composition and

structuration on metal partitioning. In a first instance, the extraction of polar solutes, namely HNO_3 and H_2O, after equilibration with aqueous phases of 1.0 and 6.0 mol L^{-1} HNO_3 in the absence of metal cation was determined for three HES compositions of x_{TOPO} from 0.3 to 0.5. The results are available in **Table S5**. Although the HNO_3 and H_2O solubilities in the HES phase are moderate, conversion of these values to molar percentages, as shown in **Figure 5**, indicates a drastic change in the nature of the HES phase particularly when considering their additional degrees of hydrogen-bonding freedom compared to $C_{10}OOH$ and TOPO. The extraction of H_2O does not significantly vary across the tested conditions, with the measured variations in HES compositions primarily induced by HNO_3 partition. Equilibrium constants (K) of the TOPO-HNO_3 extraction pair in conventional SX are in the range of $0.66 \leq \ln(K) \leq 1.28$ depending on diluting solvent,[57] reflecting the affinity of TOPO for molecular HNO_3. The extent of HNO_3 partition is dependent on the initial x_{TOPO}, i.e. the n(TOPO):n($C_{10}OOH$) ratio dictating the number of free TOPO ligands, and aqueous HNO_3 concentration. Whilst the extraction of HNO_3 varies approximately linearly with x_{TOPO} for 1.0 mol L^{-1} HNO_3, it changes to an exponential relationship at 6.0 mol L^{-1} HNO_3. For $x_{TOPO} = 0.5$, the two extraction regimes first identified in **Figure 1B**, namely a "complexation dominated" one for $[HNO_3] \leq 1.0$ mol L^{-1} to an "HNO_3 dominated" one for $[HNO_3] > 1.0$ mol L^{-1}, are clearly reflected in the n(HNO_3) to n(TOPO) ratio of **Figure 5**. Within experimental error, the 1:1 ratio of n(HNO_3):n(TOPO) obtained for an initial aqueous HNO_3 concentration of 6.0 mol L^{-1} HNO_3 suggest that TOPO(HNO_3) is now the dominant form of the ligand.

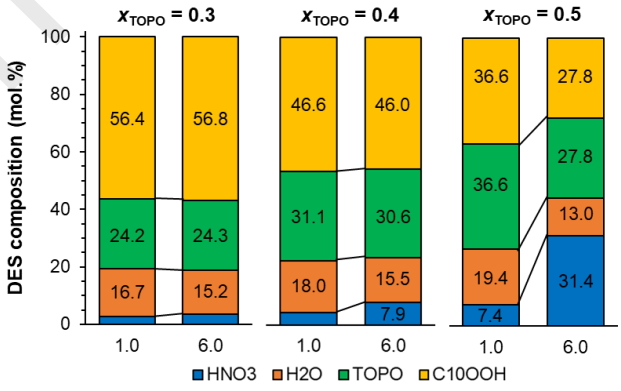

Figure 5. Initial aqueous phase HNO_3 concentration on the $C_{10}OOH$+TOPO HES phase composition at equilibrium for three x_{TOPO} values. The extracted water and acid content to the HES phase are reported in **Table S5**.

To ascertain if the change in the nature of the eutectic phase composition is reflected in its structuration and potentially on its extraction performance, the HES phase for x_{TOPO} from 0.3 to 0.5 before and after equilibration was analysed by Raman spectroscopy and SAXS. Raman analysis of the C_{10}OOH+TOPO eutectic after preparation in **Figure 6** focuses on the carboxylic region as the P=O stretch vibrations of TOPO between 1100 to 1200 cm^{-1} unfortunately overlaps with those of C_{10}OOH (*cf* **Figure S6** for the full spectra between 500 to 1800 cm^{-1}).[37] The HES spectra are further compared against that of octanoic acid as it is liquid at room temperature contrary to decanoic acid, the change from C10 to C8 alkyl chain is not expected to impact the interpretation. The carboxylic region from 1580 to 1800 cm^{-1} was deconvoluted into three contributions, namely that of the carboxylic cyclic dimer at 1660 cm^{-1} and two weaker H-bond interactions at 1716 cm^{-1} and 1734 cm^{-1}.

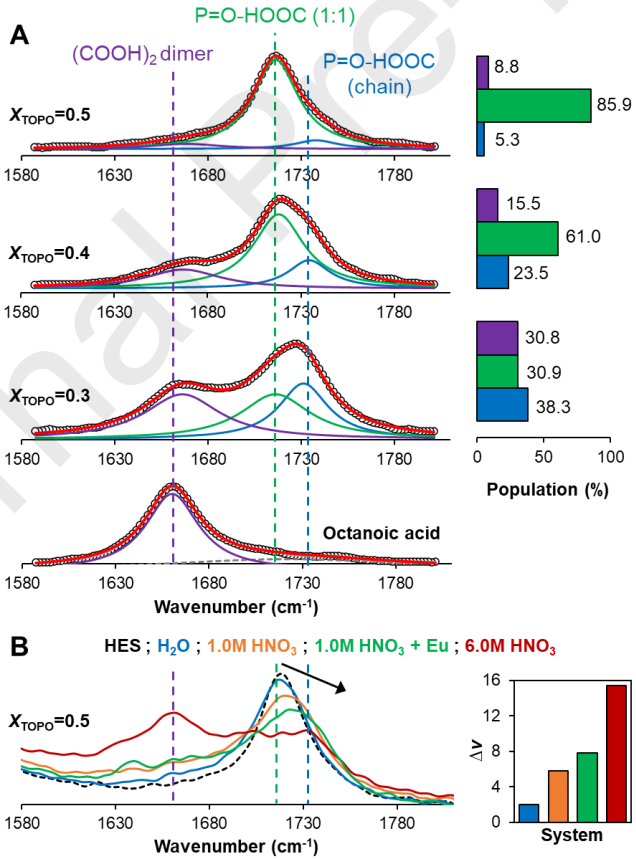

Figure 6. A) Raman analysis of the C_{10}OOH+TOPO HES after preparation showing the deconvolution of the carboxylic bands and their comparison against liquid octanoic acid. Spectra were fitted using Lorentz bands after baseline subtraction (black circles – experimental

data after baseline subtraction; red line – cumulative fit). B) Raman analysis of the $C_{10}OOH$+TOPO HES for x_{TOPO} = 0.5 after equilibration with H_2O, 1.0 and 6.0 mol L^{-1} HNO_3, and an $[Eu]_{aq,ini}$ = 0.1 mol L^{-1} solution containing 1.0 mol L^{-1} HNO_3 and 0.5 mol L^{-1} $NaNO_3$ (D_{Eu} given in **Table 1**). The shift in the HES peak at 1716 cm^{-1} with the aqueous phase composition is shown in inset (O/A = 0.5). All spectra are standardised relative to the CH_2 band at 2901 cm^{-1}.

The HES phase for x_{TOPO} = 0.5 is dominated by the band at 1716 cm^{-1} assigned to the 1:1 $C_{10}OOH$:TOPO H-bonded adduct, which gradually disappears as more $C_{10}OOH$ is added. Although a 1 to 1 association is discussed, it is important to reiterate that this is a practical simplification as liquid HES are in a dynamic equilibrium. The emergence of a red-shifted band at 1734 cm^{-1} suggests a weaking in the individual TOPO-$HOOC_{10}$ H-bond as TOPO is included as part of H-bonded oligomeric chain network where the number of hydrogen liaisons per TOPO molecule is between one to two in accordance with previous molecular dynamic simulations.[27] The results in **Figure 6A** indicate the "entrapment" of TOPO in the HES phase with decreasing x_{TOPO}, effectively raising the energetic barrier to Ln^{3+} complexation through the breakage of multiple H-bonds. The extraction of polar solutes to the HES phase (x_{TOPO} = 0.5), namely H_2O, HNO_3, and Eu^{3+}, also disrupt the 1:1 $C_{10}OOH$:TOPO H-bond as shown in **Figure 6B** and the resulting band dislocation relative to that in the pure HES at 1716 cm^{-1}. Despite the introduction of ionic interaction after Eu^{3+} extraction, the weakening of the HB association of $C_{10}OOH$ is more pronounced upon HNO_3 inclusion in the HES phase. The HES spectrum following equilibration with a 6.0 mol L^{-1} HNO_3 solution exhibits a notable band of the carboxylic dimer at 1660 cm^{-1}, confirming the liberation of $C_{10}OOH$ due to the preferential interaction of TOPO with HNO_3 and the formation of an extended H-bonded network as inferred from the COOH bands shift from 1716 cm^{-1} to 1732 cm^{-1}. The similarities between the HES phase spectra for x_{TOPO}=0.3 and x_{TOPO}=0.5 after equilibration with 6.0 mol L^{-1} HNO_3 suggest that the excess presence of strong H-bond donor, achieved through the variation in the HES HBD ratio or solute co-extraction, negatively affects the obtained D_{Ln} under these conditions due to the reduction in the number of weakly H-bonded TOPO ligands.

The internal liquid structure of the HES phase was further probed by SAXS to better understand the link between its self-organisation at the nanoscale and the macroscale properties described until now. SAXS relies on the difference in the scattering of X-rays due to the aggregation of

electron-rich molecular groups (extractant headgroups, water, acid, ions) relative to the surrounding electron-poor alkyl chains. The supramolecular organisation of the HES is rationalised based on the extensive literature addressing the liquid structure of monohydroxy alcohols with long alkyl chains such as octanol.[74,75] In such systems, a polar/apolar segregation was observed in which the presence of H-bonds bonds facilitate the transformation of small polar domains into longer H-bonded chain-like prolate clusters as illustrated in **Figure 7A**.[75–77] The resulting SAXS scattering arising from intermolecular interactions is characterized by a "pre-peak" at lower Q values related to the nano-to-mesoscale structure of the H-bond network and an "adjacency peak" at higher Q values resulting from correlations between neighbouring atoms as exemplified in **Figure 7B**. The pre-peak represents a correlation distance between the polar domains that are separated by the alkyl chains penetrating in each other. The distance between domains should be about ~1.5-1.8 time the average length of the alkyl chains as was reported for linear alcohols.[74,75] In the absence of information on the size and shape of these domains, an analytical description of the SAXS pattern in term of form and structure factor is complex and will represent the subject of a future work.

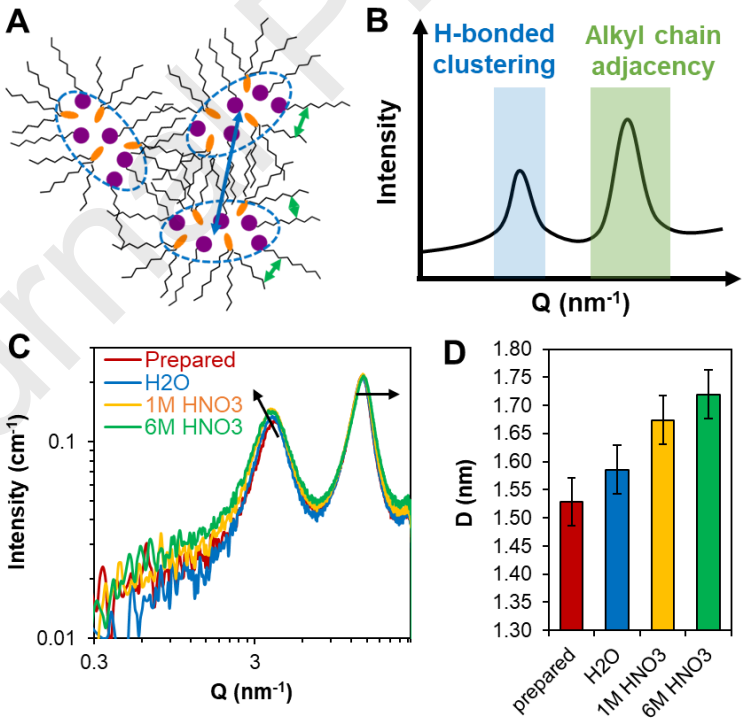

Figure 7. Simplified schematic of A) a possible mixed C_{10}OOH+TOPO cluster showing the prolate-shaped polar core and B) its manifestation as peaks in the SAXS profile. C) Scattering curves of the C_{10}OOH+TOPO HES for x_{TOPO} = 0.5 after preparation and equilibration with

H_2O, 1.0 and 6.0 mol L^{-1} HNO_3. Arrows indicate the shift in the peak position with the change in composition. D) Real space distance of the pre-peak maxima in panel C) obtained using $D = 2\pi/Q_{max}$, error bars correspond to the standard error.

The SAXS profile of the HES phase with compositions corresponding to those in **Figure 6B** and summarised in **Table S5** are presented in **Figure 7C**. A zoom of the peak regions is also provided in **Figure S7** for greater clarity. The prepared HES displays a pre-peak centred at 4.1 nm^{-1} and a second at 13.9 nm^{-1}. A similar profile was observed in the 1:1 thymol+menthol eutectic mixture albeit with a greater pre-peak Q value of 6.0 nm^{-1},[36] most likely due to the lower conformational flexibility of the components and poorer packing characteristic of the isopropane group preventing the formation of extended H-bonded chains. Converting the pre-peak position of the $C_{10}OOH$+TOPO (x_{TOPO}) = 0.5 to its real space distance given by $D = 2\pi/Q_{max}$ gives 1.53 nm. This represents approximately 1.7 times the length of the octyl alkyl chain of TOPO in a fully trans configuration (~0.9 nm), in line with previously suggested overlap of the aliphatic domains between clusters. The extraction of polar solutes (H_2O and HNO_3) and their incorporation into the HES H-bond network swells the domain size as evidenced by the broadening of the pre-peak and its shift to lower Q values as the concentration of polar solutes increases after equilibration with H_2O, 1.0 mol L^{-1} HNO_3 and finally 6.0 mol L^{-1} HNO_3. The scattering changes relative to the prepared HES are small but consistent and become more apparent when converted to the real space distance of the pre-peak maxima in **Figure 7D**. The latter clearly shows the increase in the H-bonding domain distance by ~0.2 nm in the HES after equilibration with 6.0 mol L^{-1} HNO_3 and is coherent with the inferred coordination changes by Raman of the components upon H_2O and HNO_3 extraction as their smaller size allows them to intercalate between $C_{10}OOH$ and TOPO. It is worth noting however that the pre-peak shift does not vary proportionally with the aqueous phase acidity as only small differences are observed between 1.0 and 6.0 mol L^{-1} HNO_3 (*c.f.* **Figure S7**). The SAXS data, regardless of the studied aqueous phase composition, does not present any low-Q scattering (Q < 1 nm^{-1}) thereby indicating the homogeneous dispersion of the extracted solutes in the HES phase and the absence of large-scale structural heterogeneities.

Relating these observations to Ln^{3+} extraction suggests that both the polar domain size and its composition contribute to D_{Ln}. The augmentation of the H-bond network provides a greater volume for ion solvation, lowering the barrier for extraction and yielding an initial increase in

D_{Ln} for HNO_3 concentrations between 0.1 to 1.0 mol L^{-1} irrespective of the Ln^{3+} cation. A similar justification was previously reported for the increase in Eu^{3+} and Nd^{3+} extraction using *N*,*N*′-dimethyl-*N*,*N*′-dioctylhexylethoxymalonamide (DMDOHEMA) in heptane as the HNO_3 concentration was increased to 3.0 mol L^{-1}.[41,42] However, a change in the nature of the HES polar network composition is observed from 1.0 to 6.0 mol L^{-1} HNO_3 at which $n(HNO_3) >> n(H_2O)$ (*cf.* **Figure 5**), corresponding to a decrease in D_{Ln}. The absence of domain size restriction on Ln^{3+} extraction at greater aqueous phase acidities, i.e. $r_{Polar\ domain} > r_{Ln(NO3)3}$, suggests that the relative increase in the partition of the heavy over light Ln^{3+} is attributable to the competition in TOPO coordination between Ln^{3+} and HNO_3 and varies with the charge density of Ln^{3+}. Comparison of the HES for x_{TOPO} = 0.3 under the same conditions as those reported for x_{TOPO} = 0.5 is available in **Figure S8**. Contrary to that observed in **Figure 7**, for x_{TOPO} = 0.3 the pre-peak position, centred at Q = 3.7 nm^{-1} in the prepared HES, is practically insensitive to the initial aqueous phase composition. The increased "rigidity" of the HES phase in the presence of excess $C_{10}OOH$ suppresses the growth and/or elongation of the H-bonded domains, thereby preventing the formation of polar cavities with sufficient volume to accommodate extracted Ln ions. The influence of the HES composition is reflected both in its extraction performance as well as in its pre-organisation, with the latter influencing the former.

The impact of Ln^{3+} extraction on the HES phase structure was assessed by equilibrating the HES phase for x_{TOPO} = 0.5 with aqueous solutions of 1.0 mol L^{-1} HNO_3 containing varying contents of $Eu(NO_3)_3$ (0.1 and 0.2 mol L^{-1}) and $NaNO_3$ (0.5, 1.0, and 2.0 mol L^{-1}) to yield final HES phase concentrations of 14.0, 36.3 and 75.3 g(Eu) L^{-1}. The resulting SAXS profiles are presented in **Figure 8A** and present an increase in the intensity with metal content due to the improved contrast of the electron-rich regions. More relevant, the diffractograms show the emergence of a third shoulder peak at ~6.0 nm^{-1} not found in the original HES spectra. The resulting pattern with three distinct peaks, illustrated in **Figure 8B** and experimentally evidenced in **Figure 8C** after deconvolution, is reminiscent of those observed in ionic liquids and is assigned to ion-ion correlations due the emergence of Eu^{3+} and NO_3^- charge ordering as the saturation limit of the HES is approached.[78] The introduction of electrostatic forces in the previously non-ionic HES phase results in an organisation of the aliphatic domain as shown by the linearly decreasing distance *D* of the adjacency peak with Eu^{3+} concentration in **Figure 8D**, indicating a gradual contraction between neighbouring alkyl chains. In contrast, the domain size indicated by the pre-peak does not vary until a jump of ~0.1 nm for [Eu] ≥ 36 g L^{-1} with no changes thereafter. The SAXS results indicate a restructuration of the HES phase beyond a

certain Ln^{3+} concentration, with the appearance of a charge peak above the [Eu] ≥ 36 g L^{-1} threshold suggesting the formation of an intermediate ionic network.[79] It will be interesting in a future work to correlate Eu^{3+} extraction with the HES H bonding network and to determine if the transformation of the HES supramolecular structure is also related to a sudden increase in the viscosity of the phase.

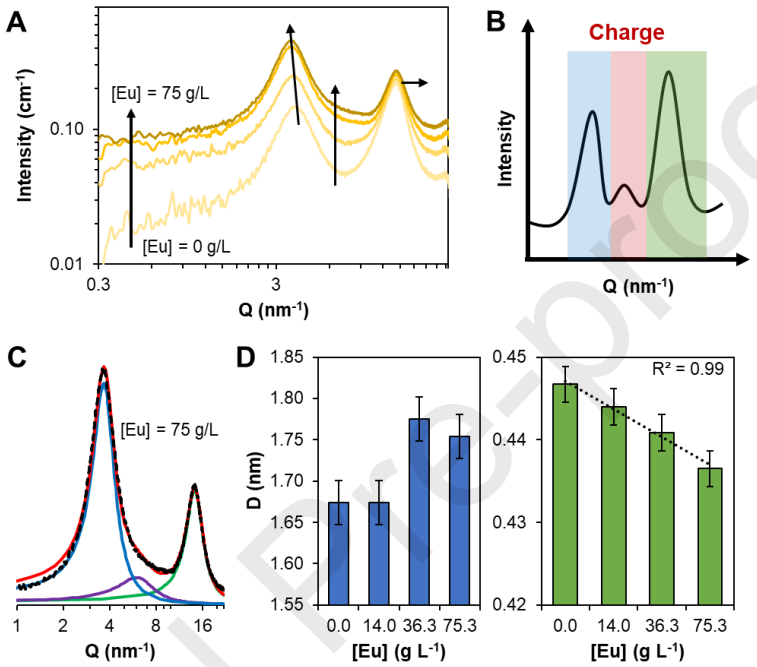

Figure 8. A) Scattering curves of the C_{10}OOH+TOPO HES for x_{TOPO} = 0.5 containing varying Eu^{3+} concentrations from 0.0 to 75.3 g L^{-1}. Extraction conditions: [HNO_3] = 1.0 mol L^{-1}; [$Eu(NO_3)_3$] = 0.1 or 0.2 mol L^{-1}, [$NaNO_3$] = 0.5, 1.0, and 2.0 mol L^{-1}; O/A = 0.5. B) Simplified schematic of the charge correlation peak in the SAXS profile. C) Example deconvolution of the HES diffractogram containing 75.3 g L^{-1} of Eu^{3+} (black circles – experimental data after baseline subtraction; red line – cumulative fit). D) Real space distance of the pre-peak (blue bars) and adjacency peak (green bars) maximum as a function of the Eu^{3+} concentration, error bars correspond to the standard error.

SX in TOPO+C_{10}OOH – Influence of temperature

In conventional SX, a detailed investigation of the extraction thermodynamic with temperature requires the confirmation of the constancy of the extraction reaction in the studied temperature range.[80] However, in the current HES system this entails not only correcting for the heat

contributions from lanthanide extraction but also considering the extraction of HNO_3 as well as accounting for the change in the HES structuration (variation in the concentration of free TOPO) due to the temperature dependency of hydrogen bonding in HES.[36] For example, it was previously shown that the Ln^{3+} partition enthalpy in the TOPO – HSCN extraction system is dependent on the total TOPO concentration.[81] As such, the potentially large cumulative uncertainties stemming from these unaccounted contributions precludes a more comprehensive study. Rather, only the gross effect of temperature on the overall extraction thermodynamics is determined by measuring the D_{Ln} as a function of temperature. The distribution of the middle (Eu^{3+}) and heavy (Lu^{3+}) lanthanides from a 1.0 mol L^{-1} HNO_3 solution were determined as a function of the temperature from 298 to 343 K and HES composition. The plotted results are presented in **Figure 9A** and **B** and the D_{Ln} values are available in **Table S4** of the ESI. To complement this, the partition of competing HNO_3 was also followed under the same extraction conditions but in the absence of Ln^{3+} ions, with the resulting distribution values shown in **Figure 9C**. Unfortunately, the large associated errors particularly at lower x_{TOPO} compositions prevented the accurate measurement of the lighter La^{3+} for comparison and as such was not included. Similarly, due to the higher associated error in D_{Eu} for greater HNO_3 concentrations, the same study at 6.0 mol L^{-1} HNO_3 was not attempted at this time.

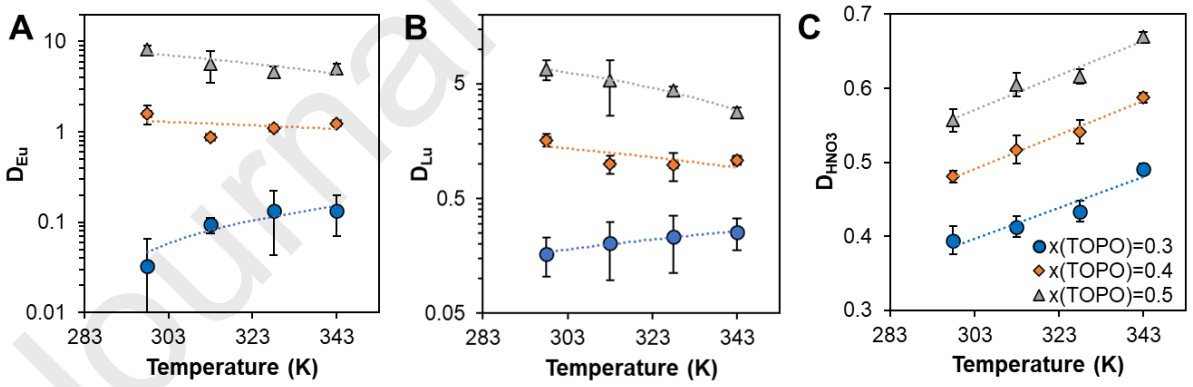

Figure 9. Temperature and x_{TOPO} molar fraction influence on the distribution of A) Eu^{3+}, B) Lu^{3+} and C) HNO_3 distribution ([HNO_3] = 1.0 mol L^{-1}, [Ln^{3+}] = 7.5 mmol L^{-1} and O/A = 0.5). All D values are available in **Table S4**.

For $x_{TOPO} \geq 0.4$, the decrease of the D_{Ln} values for both Eu^{3+} and Lu^{3+} with the temperature indicates an exothermic extraction process. Interestingly, an inverse D_{Ln} tendency was

observed at a lower TOPO molar fraction of 0.3 for both Ln^{3+} indicative of an endothermic extraction process. The inversion from an exothermic to endothermic Ln^{3+} extraction with decreasing x_{TOPO} cannot be rationalised based on HNO_3 co-extraction as similar temperature dependent D_{HNO3} profiles were obtained for all studied HES compositions as shown in **Figure 9C**. Notably, the endothermic nature of HNO_3 extraction by HES in the absence of metal is contrary to that obtained using 0.05 mol L^{-1} TOPO diluted in heptane for which an exothermic extraction enthalpy of ΔH= -14.6 kJ mol^{-1} was reported.[57] As such, a potential explanation as to the change in D_{Ln} tendency with decreasing x_{TOPO} could be due to the greater contribution of $C_{10}OOH$ to the extraction as linear and aromatic carboxylic and dicarboxylic acids all typically present positive enthalpies of complexation with Ln^{3+}.[82,83] The apparent extraction thermodynamic parameters, representing an amalgamation of all processes occurring in parallel with to Ln^{3+} extraction, were determined by plotting the Gibbs free energies of transfer for Eu^{3+} and Lu^{3+} as a function of temperature and x_{TOPO}, with the results presented in **Figure S9**. Considering the simplifying assumptions made, the corresponding calculated enthalpy and entropy values, summarised in **Table 2,** should be regarded on a comparative basis rather than quantitative values. Similar ΔH and ΔS values as in **Table 2** were also obtained when using the van't Hoff formalism by plotting $Ln(D_{Ln})$ vs. $1/T$ (K^{-1}) assuming that D_{Ln} is proportional to a composite-equilibrium constant for the overall extraction.

Table 2. Values of measured values of measured entropy (ΔS) and enthalpy (ΔH) derived from the slope and intercept respectively of the curves in **Figure S7** of the ESI.

x_{TOPO}	Eu^{3+}			Lu^{3+}			HNO_3		
	0.3	**0.4**	**0.5**	**0.3**	**0.4**	**0.5**	**0.3**	**0.4**	**0.5**
ΔH (kJ mol^{-1})	23.3	-2.5	-8.6	8.9	-6.7	-15.2	3.6	3.7	3.3
ΔS (J K^{-1} mol^{-1})	51.9	-6.4	-12.4	14.0	-20.0	-35.2	-4.5	-6.3	-6.1

The obtained ΔH values in HES are two to three times smaller than in the comparable traditional SX, possibly reflecting the increased energetic disadvantage when TOPO acts both as the extractant and HES phase former. In the conventional SX system composed of 0.2 mol L^{-1} TOPO in toluene and an aqueous phase of 0.1 mol L^{-1} HNO_3 with 3.9 mol L^{-1} $NaNO_3$, ΔH remains approximately constant across the Ln^{3+} series at around –29.0 kJ mol^{-1} until Er(III) and increases slightly for the heaviest Ln.[84] In contrast, Lu^{3+} consistently presents a more

negative Δ*H* value than Eu^{3+} across all HES compositions. However, the larger Δ*H* is offset by a greater entropic penalty as is apparent when considering the 1.2-fold stronger extraction of Eu^{3+} relative to Lu^{3+} for 1.0 mol L^{-1} HNO_3 and x_{TOPO}=0.5 (**Figure 1**), representing an energetic contribution of $\Delta(\Delta G) = -RT\ln(1.2) = -0.5$ kJ mol^{-1}. In fact, the linear dependency of the extraction Δ*H* with Δ*S* as shown in **Figure S10** suggests the occurrence of an enthalpy–entropy compensation for Ln^{3+} extraction from nitrate media using the TOPO+C_{10}OOH HES. A similar compensation effect was observed between Ln^{3+} and ligands containing hard donor atoms,[80] including TOPO.[85] Differing from the enthalpy-driven nature of Ln^{3+} extraction with TOPO[81,84] and most extractants[80] in conventional SX, entropy appears to play a more significant role in SX in HES as $|\Delta G_R| \leq |-T\Delta S|$ for most x_{TOPO} and temperature combinations. As expected from the results in **Figure 9C**, within experimental error no difference in Δ*H* and Δ*S* values for the apparent extraction of HNO_3 was observed as a function of x_{TOPO}. Whilst a more systematic and detailed thermodynamic study is required, the obtained results and their difference with traditional SX suggest the dominant role of the intermolecular HES phase interaction on the extraction that should be explicitly considered.

CONCLUSIONS

In this work, the extraction of lanthanides from nitrate media by the non-ideal solvent composed of C_{10}OOH+TOPO was determined as a function of the lanthanide cation selection, HES molar fraction, HNO_3 concentration, and temperature. Special emphasis was placed on the determination of the relationship between the HES phase structuration and the extraction performance. A compromise between maximum Ln^{3+} loading and selectivity was observed, driven by the variation in the quantity of weakly H-bonded TOPO and the change in the configurational entropy of the mixture. A maximum distribution for all lanthanides was observed for an aqueous phase acidity of 0.5 to 1.0 mol L^{-1} HNO_3 with a preference for Eu^{3+}, resulting in a sharp break in D_{Ln} between the adjacent Eu^{3+} and Gd^{3+} to yield an interesting $SF_{Eu/Gd}$ of 1.8. The D_{Ln} decreased both with increased HNO_3 concentrations and C_{10}OOH content. However, this decrease was more pronounced for the light and middle Ln, allowing for a change in the extraction selectivity and a $SF_{Lu/La}$ of 115 at 4.0 mol L^{-1} HNO_3. The selectivity could be further tuned through the variation in x_{TOPO} but again at the expense of the maximum achievable D_{Ln}. Overall, the studied HES presented good D_{Ln} values across a range of acidities and exhibited a comparable selectivity to classical SX systems using non-ionic

extractants whilst eliminating the need for volatile diluents and phase modifiers. Spectroscopic and SAXS analysis indicate that the change in extraction with x_{TOPO} and/or HNO_3 concentration is due to the modification of the HES phase composition and organisation rather than a change in the extracted complex. All results point towards the need to explicitly consider the HES phase structuration and its compositional changes with solute co-extraction on the Ln^{3+} extraction, which should vary based on the "deepness" (i.e. strength of intermolecular interaction) of the HES mixture. It is expected that the presented conclusions are extrapolable to other possible HES combinations presenting a non-ideal behaviour for the extraction of metal ions and polar solutes. Looking beyond the scope of this work, HES appear as promising model solvents to explore the role of H-bonding interactions in complex liquid phases and their link to SX. Further work is required to identify suitable washing and stripping solutions capable of improving on the lanthanide separation whilst regenerating the HES phase without provoking a modification of its original HBD to HBA molar ratio.

ACKOWLEDGMENTS

This work was partly developed within the scope of the project CICECO-Aveiro Institute of Materials, UIDB/50011/2020, UIDP/50011/2020, and LA/P/0006/2020, financed by national funds through the FCT/MCTES. This work was supported by the Instituto Nacional de Ciências e Tecnologias Analíticas Avançadas (INCTAA)/Conselho Nacional de Desenvolvimento Científico e Tecnológico (CNPq) [grant number 465768/2014-8]; Fundação de Amparo à Pesquisa do Estado de Minas Gerais (FAPEMIG) [grant number CEX-PPM-00585-17]; CNPq [grant number 305649/2021-3, 131790/2020-0]; Coordenação de Aperfeiçoamento de Pessoal de Nível Superior (CAPES)/Fundação para a Ciência e Tecnologia (FCT) [grant number 88881.309048/2018-01]; CAPES [grant number 88882.437092/2019-01].

REFERENCES

(1) Reck, B. K.; Graedel, T. E. Challenges in Metal Recycling. *Science.* **2012**, *337* (6095), 690–695. https://doi.org/10.1126/science.1217501.

(2) Adrian, S.; Drisse, M. B.; Cheng, Y.; Devia, L.; Deubzer, O.; Goldizen, F.; Gorman, J.; Herat, S.; Honda, S.; Iattoni, G.; Jingwei, W.; Jinhui, L.; Khetriwal, D. S.; Linnell, J.; Magalini, F.; Nnororm, I. C.; Onianwa, P.; Ott, D.; Ramola, A.; Silva, U.; Stillhart, R.; Tillekeratne, D.; Van Straalen, V.; Wagner, M.; Yamamoto, T.; Zeng, X. *The Global E-Waste Monitor 2020: Quantities, Flows, and the Circular Economy Potential*;

Bonn/Geneva/Rotterdam, 2020.

(3) Cui, J.; Zhang, L. Metallurgical Recovery of Metals from Electronic Waste: A Review. *J. Hazard. Mater.* **2008**, *158* (2–3), 228–256. https://doi.org/10.1016/j.jhazmat.2008.02.001.

(4) Wilson, A. M.; Bailey, P. J.; Tasker, P. A.; Turkington, J. R.; Grant, R. A.; Love, J. B. Solvent Extraction: The Coordination Chemistry behind Extractive Metallurgy. *Chem. Soc. Rev.* **2013**, *43* (1), 123–134. https://doi.org/10.1039/C3CS60275C.

(5) Xie, F.; Zhang, T. A.; Dreisinger, D.; Doyle, F. A Critical Review on Solvent Extraction of Rare Earths from Aqueous Solutions. *Miner. Eng.* **2014**, *56*, 10–28. https://doi.org/10.1016/j.mineng.2013.10.021.

(6) Sholl, D. S.; Lively, R. P. Seven Chemical Separations to Change the World. *Nature* **2016**, *532*, 435–437. https://doi.org/https://doi.org/10.1038/532435a.

(7) Nash, K. L. A Review of the Basic Chemistry and Recent Developments in Trivalent F-Elements Separations. *Solvent Extr. Ion Exch.* **1993**, *11* (4), 729–768. https://doi.org/10.1080/07366299308918184.

(8) Peters, J. A.; Djanashvili, K.; Geraldes, C. F. G. C.; Platas-Iglesias, C. The Chemical Consequences of the Gradual Decrease of the Ionic Radius along the Ln-Series. *Coord. Chem. Rev.* **2020**, *406*, 213146. https://doi.org/10.1016/J.CCR.2019.213146.

(9) Cheisson, T.; Schelter, E. J. Rare Earth Elements: Mendeleev's Bane, Modern Marvels. *Science*. **2019**, 489–493. https://doi.org/10.1126/science.aau7628.

(10) Shannon, R. D. Revised Effective Ionic Radii and Systematic Studies of Interatomic Distances in Halides and Chalcogenides. *Acta Crystallogr. Sect. A* **1976**, *32* (5), 751–767. https://doi.org/10.1107/S0567739476001551.

(11) Roca-Sabio, A.; Mato-Iglesias, M.; Esteban-Gómez, D.; Toth, É.; De Bias, A.; Platas-Iglesias, C.; Rodríguez-Blas, T. Macrocyclic Receptor Exhibiting Unprecedented Selectivity for Light Lanthanides. *J. Am. Chem. Soc.* **2009**, *131* (9), 3331–3341. https://doi.org/10.1021/ja808534w.

(12) Nomizu, D.; Sasaki, Y.; Kaneko, M.; Matsumiya, M.; Katsuta, S. Complex Formation of Light and Heavy Lanthanides with DGA and DOODA, and Its Application to Mutual Separation in DGA–DOODA Extraction System. *J. Radioanal. Nucl. Chem.* **2022**, *331* (3), 1483–1493. https://doi.org/10.1007/S10967-022-08204-5.

(13) Vahidi, E.; Zhao, F. Environmental Life Cycle Assessment on the Separation of Rare Earth Oxides through Solvent Extraction. *J. Environ. Manage.* **2017**, *203*, 255–263. https://doi.org/10.1016/j.jenvman.2017.07.076.

(14) Abranches, D. O.; Martins, M. A. R.; Silva, L. P.; Schaeffer, N.; Pinho, S. P.; Coutinho, J. A. P. Phenolic Hydrogen Bond Donors in the Formation of Non-Ionic Deep Eutectic Solvents: The Quest for Type v Des. *Chem. Commun.* **2019**, *55* (69), 10253–10256. https://doi.org/10.1039/c9cc04846d.

(15) Martins, M. A. R.; Pinho, S. P.; Coutinho, J. A. P. Insights into the Nature of Eutectic and Deep Eutectic Mixtures. *J. Solution Chem.* **2019**, *48* (7), 962–982. https://doi.org/10.1007/s10953-018-0793-1.

(16) Edgecomb, J. M.; Tereshatov, E. E.; Zante, G.; Boltoeva, M.; Folden, C. M.

Hydrophobic Amine-Based Binary Mixtures of Active Pharmaceutical and Food Grade Ingredients: Characterization and Application in Indium Extraction from Aqueous Hydrochloric Acid Media. *Green Chem.* **2020**, *22* (20), 7047–7058. https://doi.org/10.1039/d0gc02452j.

(17) Byrne, E. L.; O'Donnell, R.; Gilmore, M.; Artioli, N.; Holbrey, J. D.; Swadźba-Kwaśny, M. Hydrophobic Functional Liquids Based on Trioctylphosphine Oxide (TOPO) and Carboxylic Acids. *Phys. Chem. Chem. Phys.* **2020**, *22* (42), 24744–24763. https://doi.org/10.1039/d0cp02605k.

(18) Schaeffer, N.; Conceição, J. H. F.; Martins, M. A. R.; Neves, M. C.; Pérez-Sánchez, G.; Gomes, J. R. B.; Papaiconomou, N.; Coutinho, J. A. P. Non-Ionic Hydrophobic Eutectics-Versatile Solvents for Tailored Metal Separation and Valorisation. *Green Chem.* **2020**, *22*, 2810–2820. https://doi.org/10.1039/d0gc00793e.

(19) Schaeffer, N.; Martins, M. A. R.; Neves, C. M. S. S.; Pinho, S. P.; Coutinho, J. A. P. Sustainable Hydrophobic Terpene-Based Eutectic Solvents for the Extraction and Separation of Metals. *Chem. Commun.* **2018**, *54* (58), 8104–8107. https://doi.org/10.1039/c8cc04152k.

(20) Gilmore, M.; McCourt, É. N.; Connolly, F.; Nockemann, P.; Swadźba-Kwaśny, M.; Holbrey, J. D. Hydrophobic Deep Eutectic Solvents Incorporating Trioctylphosphine Oxide: Advanced Liquid Extractants. *ACS Sustain. Chem. Eng.* **2018**, *6* (12), 17323–17332. https://doi.org/10.1021/acssuschemeng.8b04843.

(21) Tereshatov, E. E.; Boltoeva, M. Y.; Folden, C. M. First Evidence of Metal Transfer into Hydrophobic Deep Eutectic and Low-Transition-Temperature Mixtures: Indium Extraction from Hydrochloric and Oxalic Acids. *Green Chem.* **2016**, *18* (17), 4616–4622. https://doi.org/10.1039/c5gc03080c.

(22) Hanada, T.; Goto, M. Synergistic Deep Eutectic Solvents for Lithium Extraction. *ACS Sustain. Chem. Eng.* **2021**, *9* (5), 2152–2160. https://doi.org/10.1021/acssuschemeng.0c07606.

(23) Almustafa, G.; Sulaiman, R.; Kumar, M.; Adeyemi, I.; Arafat, H. A.; AlNashef, I. Boron Extraction from Aqueous Medium Using Novel Hydrophobic Deep Eutectic Solvents. *Chem. Eng. J.* **2020**, *395*, 125173. https://doi.org/10.1016/J.CEJ.2020.125173.

(24) Ni, S.; Gao, Y.; Yu, G.; Zhang, S.; Zeng, Z.; Sun, X. Tailored Ternary Hydrophobic Deep Eutectic Solvents for Synergistic Separation of Yttrium from Heavy Rare Earth Elements. *Green Chem.* **2022**, *24* (18), 7148–7161. https://doi.org/10.1039/D2GC02566C.

(25) Abbott, A. P.; Capper, G.; Davies, D. L.; Rasheed, R. K.; Tambyrajah, V. Novel Solvent Properties of Choline Chloride/Urea Mixtures. *Chem. Commun.* **2003**, 1, 70–71. https://doi.org/10.1039/b210714g.

(26) Peloquin, A. J.; McCollum, J. M.; McMillen, C. D.; Pennington, W. T. Halogen Bonding in Dithiane/Iodofluorobenzene Mixtures: A New Class of Hydrophobic Deep Eutectic Solvents. *Angew. Chemie Int. Ed.* **2021**, *60* (42), 22983–22989. https://doi.org/10.1002/ANIE.202110520.

(27) Vargas, S. J. R.; Pérez-Sánchez, G.; Schaeffer, N.; Coutinho, J. A. P. Solvent Extraction in Extended Hydrogen Bonded Fluids – Separation of Pt(IV) from Pd(II) Using TOPO-Based Type V DES. *Green Chem.* **2021**, *23* (12), 4540–4550.

https://doi.org/10.1039/D1GC00829C.

(28) van den Bruinhorst, A.; Raes, S.; Maesara, S. A.; Kroon, M. C.; Esteves, A. C. C.; Meuldijk, J. Hydrophobic Eutectic Mixtures as Volatile Fatty Acid Extractants. *Sep. Purif. Technol.* **2019**, *216*, 147–157. https://doi.org/10.1016/j.seppur.2018.12.087.

(29) Kaul, M. J.; Mandella, V.; Dietz, M. L. Systematic Evaluation of Hydrophobic Deep Eutectic Solvents as Alternative Media for the Extraction of Metal Ions from Aqueous Solution. *Talanta* **2022**, *243*, 123373. https://doi.org/10.1016/j.talanta.2022.123373.

(30) Bourgeois, D.; El Maangar, A.; Dourdain, S. Importance of Weak Interactions in the Formulation of Organic Phases for Efficient Liquid/Liquid Extraction of Metals. *Curr. Opin. Colloid Interface Sci.* **2020**, *46*, 36–51. https://doi.org/10.1016/J.COCIS.2020.03.004.

(31) Špadina, M.; Dufrêche, J. F.; Pellet-Rostaing, S.; Marčelja, S.; Zemb, T. Molecular Forces in Liquid-Liquid Extraction. *Langmuir* **2021**, *37* (36), 10637–10656. https://doi.org/10.1021/ACS.LANGMUIR.1C00673.

(32) Motokawa, R.; Kobayashi, T.; Endo, H.; Mu, J.; Williams, C. D.; Masters, A. J.; Antonio, M. R.; Heller, W. T.; Nagao, M. A Telescoping View of Solute Architectures in a Complex Fluid System. *ACS Cent. Sci.* **2019**, *5* (1), 85–96. https://doi.org/10.1021/acscentsci.8b00669.

(33) Špadina, M.; Bohinc, K.; Zemb, T.; Dufrêche, J. F. Synergistic Solvent Extraction Is Driven by Entropy. *ACS Nano* **2019**, *13* (12), 13745–13758. https://doi.org/10.1021/acsnano.9b07605.

(34) Rey, J.; Dourdain, S.; Dufrêche, J. F.; Berthon, L.; Muller, J. M.; Pellet-Rostaing, S.; Zemb, T. Thermodynamic Description of Synergy in Solvent Extraction: I. Enthalpy of Mixing at the Origin of Synergistic Aggregation. *Langmuir* **2016**, *32* (49), 13095–13105. https://doi.org/10.1021/acs.langmuir.6b02343.

(35) Rey, J.; Dourdain, S.; Berthon, L.; Jestin, J.; Pellet-Rostaing, S.; Zemb, T. Synergy in Extraction System Chemistry: Combining Configurational Entropy, Film Bending, and Perturbation of Complexation. *Langmuir* **2015**, *31* (25), 7006–7015. https://doi.org/10.1021/ACS.LANGMUIR.5B01478.

(36) Schaeffer, N.; Abranches, D. O.; Silva, L. P.; Martins, M. A. R.; Carvalho, P. J.; Russina, O.; Triolo, A.; Paccou, L.; Guinet, Y.; Hedoux, A.; Coutinho, J. A. P. Non-Ideality in Thymol + Menthol Type V Deep Eutectic Solvents. *ACS Sustain. Chem. Eng.* **2021**. https://doi.org/10.1021/acssuschemeng.0c07874.

(37) Tkac, P.; Vandegrift, G. F.; Lumetta, G. J.; Gelis, A. V. Study of the Interaction between HDEHP and CMPO and Its Effect on the Extraction of Selected Lanthanides. *Ind. Eng. Chem. Res.* **2012**, *51* (31), 10433–10444. https://doi.org/10.1021/ie300326d.

(38) Servis, M. J.; Stephenson, G. B. Mesostructuring in Liquid-Liquid Extraction Organic Phases Originating from Critical Points. *J. Phys. Chem. Lett.* **2021**, *12*, 5807–5812. https://doi.org/10.1021/acs.jpclett.1c01429.

(39) Baldwin, A. G.; Ivanov, A. S.; Williams, N. J.; Ellis, R. J.; Moyer, B. A.; Bryantsev, V. S.; Shafer, J. C. Outer-Sphere Water Clusters Tune the Lanthanide Selectivity of Diglycolamides. *ACS Cent. Sci.* **2018**, *4* (6), 739–747. https://doi.org/10.1021/acscentsci.8b00223.

(40) Brigham, D. M.; Ivanov, A. S.; Moyer, B. A.; Delmau, L. H.; Bryantsev, V. S.; Ellis, R. J. Trefoil-Shaped Outer-Sphere Ion Clusters Mediate Lanthanide(III) Ion Transport with Diglycolamide Ligands. *J. Am. Chem. Soc.* **2017**, *139* (48), 17350–17358. https://doi.org/10.1021/JACS.7B07318.

(41) Qiao, B.; Demars, T.; Olvera De La Cruz, M.; Ellis, R. J. How Hydrogen Bonds Affect the Growth of Reverse Micelles around Coordinating Metal Ions. *J. Phys. Chem. Lett.* **2014**, *5* (8), 1440–1444. https://doi.org/10.1021/JZ500495P.

(42) Poirot, R.; Le Goff, X.; Diat, O.; Bourgeois, D.; Meyer, D. Metal Recognition Driven by Weak Interactions: A Case Study in Solvent Extraction. *ChemPhysChem* **2016**, *17* (14), 2112–2117. https://doi.org/10.1002/CPHC.201600305.

(43) Artese, A.; Dourdain, S.; Boubals, N.; Dumas, T.; Solari, P. L.; Menut, D.; Berthon, L.; Guilbaud, P.; Pellet-Rostaing, S. Evidence of Supramolecular Origin of Selectivity in Solvent Extraction of Bifunctional Amidophosphonate Extractants with Different Configurations. *Solvent Extr. Ion Exch.* **2021**, *40* (4), 431–453. https://doi.org/10.1080/07366299.2021.1961433.

(44) Lu, Z.; Dourdain, S.; Pellet-Rostaing, S. Understanding the Effect of the Phase Modifier N-Octanol on Extraction, Aggregation, and Third-Phase Appearance in Solvent Extraction. *Langmuir* **2020**, *36* (41), 12121–12129. https://doi.org/10.1021/acs.langmuir.0c01554.

(45) Mathur, J. N.; Choppin, G. R. Paraffin Wax - TOPO, an Extractant for Actinides and Lanthanides. *Solvent Extr. Ion Exch.* **1997**, *16* (3), 739–749. https://doi.org/10.1080/07366299808934550.

(46) Gupta, B.; Malik, P.; Deep, A. Solvent Extraction and Separation of Tervalent Lanthanides and Yttrium Using Cyanex 923. *Solvent Extr. Ion Exch.* **2003**, *21* (2), 239–258. https://doi.org/10.1081/SEI-120018948.

(47) Tunsu, C.; Ekberg, C.; Foreman, M.; Retegan, T. Studies on the Solvent Extraction of Rare Earth Metals from Fluorescent Lamp Waste Using Cyanex 923. *Solvent Extr. Ion Exch.* **2014**, *32* (6), 650–668. https://doi.org/10.1080/07366299.2014.925297.

(48) Lommelen, R.; Binnemans, K. Hard-Soft Interactions in Solvent Extraction with Basic Extractants: Comparing Zinc and Cadmium Halides. *ACS Omega* **2021**, *6* (42), 27924–27935. https://doi.org/10.1021/acsomega.1c03790.

(49) Platt, A. W. G. Lanthanide Phosphine Oxide Complexes. *Coord. Chem. Rev.* **2017**, *340*, 62–78. https://doi.org/10.1016/J.CCR.2016.09.012.

(50) du Preez, A. C.; Preston, J. S. The Solvent Extraction of Rare-Earth Metals by Carboxylic Acids. *Solvent Extr. Ion Exch.* **2007**, *10* (2), 207–230. https://doi.org/10.1080/07366299208918101.

(51) Dourdain, S.; Hofmeister, I.; Pecheur, O.; Dufrêche, J. F.; Turgis, R.; Leydier, A.; Jestin, J.; Testard, F.; Pellet-Rostaing, S.; Zemb, T. Synergism by Coassembly at the Origin of Ion Selectivity in Liquid-Liquid Extraction. *Langmuir* **2012**, *28* (31), 11319–11328. https://doi.org/10.1021/la301733r.

(52) Dangelo, P.; Zitolo, A.; Migliorati, V.; Chillemi, G.; Duvail, M.; Vitorge, P.; Abadie, S.; Spezia, R. Revised Ionic Radii of Lanthanoid(III) Ions in Aqueous Solution. *Inorg. Chem.* **2011**, *50* (10), 4572–4579. https://doi.org/10.1021/IC200260R.

(53) Duvail, M.; Ruas, A.; Venault, L.; Moisy, P.; Guilbaud, P. Molecular Dynamics Studies of Concentrated Binary Aqueous Solutions of Lanthanide Salts: Structures and Exchange Dynamics. *Inorg. Chem.* **2010**, *49* (2), 519–530. https://doi.org/10.1021/IC9017085.

(54) Yaita, T.; Narita, H.; Suzuki, S.; Tachimori, S.; Motohashi, H.; Shiwaku, H. Structural Study of Lanthanides(III) in Aqueous Nitrate and Chloride Solutions by EXAFS. *J. Radioanal. Nucl. Chem. 1999 2392* **1999**, *239* (2), 371–375. https://doi.org/10.1007/BF02349514.

(55) Alguacil, F. J.; López, F. A. The Extraction of Mineral Acids by the Phosphine Oxide Cyanex 923. *Hydrometallurgy* **1996**, *42* (2), 245–255. https://doi.org/10.1016/0304-386X(95)00101-L.

(56) Bucher, J. J.; Conocchioli, T. J.; Held, E. R.; Labinger, J. A.; Sudbury, B. A.; Diamond, R. M. Extraction of HReO4, HNO3, HBr and HCl by Trioctylphosphine Oxide in Nitrobenzene and in 1,2-Dichloroethane, and Hydration of the Anions. *J. Inorg. Nucl. Chem.* **1975**, *37* (1), 221–227. https://doi.org/10.1016/0022-1902(75)80154-0.

(57) Petkovlć, D. M. .; Kopečni, M. M. .; Mltrovlć, & A. A. Solvent Extraction of Nitric, Hydrochloric and Sulfuric Acid and Their Uranyl Salts with Tri-n-Octylphosphine Oxide. *Solvent Extr. Ion Exch.* **1992**, *10* (4), 685–696. https://doi.org/10.1080/07366299208918129.

(58) Ruas, A.; Pochon, P.; Simonin, J.-P.; Moisy, P. Nitric Acid: Modeling Osmotic Coefficients and Acid-Base Dissociation Using the BIMSA Theory † ‡. **2010**. https://doi.org/10.1039/c0dt00343c.

(59) Mu, J.; Motokawa, R.; Akutsu, K.; Nishitsuji, S.; Masters, A. J. A Novel Microemulsion Phase Transition: Toward the Elucidation of Third-Phase Formation in Spent Nuclear Fuel Reprocessing. *J. Phys. Chem. B* **2018**, *122* (4), 1439–1452. https://doi.org/10.1021/acs.jpcb.7b08515.

(60) Peppard, D. F.; Bloomquist, C. A. A.; Horwitz, E. P.; Lewey, S.; Mason, G. W. Analogous Actinide (III) and Lanthanide (III) Tetrad Effects. *J. Inorg. Nucl. Chem.* **1970**, *32* (1), 339–343. https://doi.org/10.1016/0022-1902(70)80478-X.

(61) Persson, I.; D'Angelo, P.; De Panfilis, S.; Sandström, M.; Eriksson, L. Hydration of Lanthanoid(III) Ions in Aqueous Solution and Crystalline Hydrates Studied by EXAFS Spectroscopy and Crystallography: The Myth of the "Gadolinium Break." *Chem. – A Eur. J.* **2008**, *14* (10), 3056–3066. https://doi.org/10.1002/CHEM.200701281.

(62) Shiery, R. C.; Fulton, J. L.; Balasubramanian, M.; Nguyen, M. T.; Lu, J. B.; Li, J.; Rousseau, R.; Glezakou, V. A.; Cantu, D. C. Coordination Sphere of Lanthanide Aqua Ions Resolved with Ab Initio Molecular Dynamics and X-Ray Absorption Spectroscopy. *Inorg. Chem.* **2021**, *60* (5), 3117–3130. https://doi.org/10.1021/ACS.INORGCHEM.0C03438.

(63) Bowden, A.; Singh, K.; Platt, A. W. G. Lanthanide Nitrate Complexes with Triethylphosphine Oxide. Solid State and Solution Properties. *Polyhedron* **2012**, *42* (1), 30–35. https://doi.org/10.1016/J.POLY.2012.04.021.

(64) Bednarczyk, L.; Siekierski, S. Extraction of Light Lanthanide Nitrates by Tri-n-Butyl Phosphate. *Solvent Extr. Ion Exch.* **1989**, *7* (2), 273–287. https://doi.org/10.1080/07360298908962309.

(65) Peppard, D. F.; Driscoll, W. J.; Sironen, R. J.; McCarty, S. Nonmonotonic Ordering of Lanthanides in Tributyl Phosphate-Nitric Acid Extraction Systems. *J. Inorg. Nucl. Chem.* **1957**, *4* (5–6), 326–333. https://doi.org/10.1016/0022-1902(57)80015-3.

(66) Reddy, M. L. P.; Luxmi Varma, R.; Ramamohan, T. R.; Sahu, S. K.; Chakravortty, V. Cyanex 923 as an Extractant for Trivalent Lanthanides and Yttrium. *Solvent Extr. Ion Exch.* **1998**, *16* (3), 795–812. https://doi.org/10.1080/07366299808934553.

(67) Sasaki, Y.; Sugo, Y.; Suzuki, S.; Tachimori, S. The Novel Extractants, Diglycolamides, for the Extraction of Lanthanides and Actinides in HNO3–n-Dodecane System. *Solvent Extr. Ion Exch.* **2000**, *19* (1), 91–103. https://doi.org/10.1081/SEI-100001376.

(68) Rout, A.; Binnemans, K. Influence of the Ionic Liquid Cation on the Solvent Extraction of Trivalent Rare-Earth Ions by Mixtures of Cyanex 923 and Ionic Liquids. *Dalt. Trans.* **2014**, *44* (3), 1379–1387. https://doi.org/10.1039/C4DT02766C.

(69) Antonio, M. R.; Ellis, R. J.; Estes, S. L.; Bera, M. K. Structural Insights into the Multinuclear Speciation of Tetravalent Cerium in the Tri-n-Butyl Phosphate–n-Dodecane Solvent Extraction System. *Phys. Chem. Chem. Phys.* **2017**, *19* (32), 21304–21316. https://doi.org/10.1039/C7CP03350H.

(70) Demars, T. J.; Bera, M. K.; Seifert, S.; Antonio, M. R.; Ellis, R. J. Revisiting the Solution Structure of Ceric Ammonium Nitrate. *Angew. Chemie Int. Ed.* **2015**, *54* (26), 7534–7538. https://doi.org/10.1002/anie.201502336.

(71) Binnemans, K. Interpretation of Europium(III) Spectra. *Coord. Chem. Rev.* **2015**, *295*, 1–45. https://doi.org/10.1016/J.CCR.2015.02.015.

(72) Supkowski, R. M.; Horrocks, W. D. W. On the Determination of the Number of Water Molecules, q, Coordinated to Europium(III) Ions in Solution from Luminescence Decay Lifetimes. *Inorganica Chim. Acta* **2002**, *340*, 44–48. https://doi.org/10.1016/S0020-1693(02)01022-8.

(73) Horrocks, W. D. W.; Sudnick, D. R. Time-Resolved Europium(III) Excitation Spectroscopy: A Luminescence Probe of Metal Ion Binding Sites. *Science.* **1979**, *206* (4423), 1194–1196. https://doi.org/10.1126/SCIENCE.505007.

(74) Böhmer, R.; Gainaru, C.; Richert, R. Structure and Dynamics of Monohydroxy Alcohols-Milestones Towards Their Microscopic Understanding, 100 Years After Debye. *Physics Reports*. Elsevier B.V. 2014, pp 125–195. https://doi.org/10.1016/j.physrep.2014.07.005.

(75) MacCallum, J. L.; Tieleman, D. P. Structures of Neat and Hydrated 1-Octanol from Computer Simulations. *J. Am. Chem. Soc.* **2002**, *124* (50), 15085–15093. https://doi.org/10.1021/JA027422O.

(76) Qiao, B.; Littrell, K. C.; Ellis, R. J. Liquid Worm-like and Proto-Micelles: Water Solubilization in Amphiphile–Oil Solutions. *Phys. Chem. Chem. Phys.* **2018**, *20* (18), 12908–12915. https://doi.org/10.1039/C8CP00600H.

(77) Sillrén, P.; Swenson, J.; Mattsson, J.; Bowron, D.; Matic, A. The Temperature Dependent Structure of Liquid 1-Propanol as Studied by Neutron Diffraction and EPSR Simulations. *J. Chem. Phys.* **2013**, *138* (21), 214501. https://doi.org/10.1063/1.4807863.

(78) Russina, O.; Lo Celso, F.; Plechkova, N. V.; Triolo, A. Emerging Evidences of Mesoscopic-Scale Complexity in Neat Ionic Liquids and Their Mixtures. *J. Phys. Chem.*

Lett. **2017**, *8* (6), 1197–1204. https://doi.org/10.1021/ACS.JPCLETT.6B02811.

(79) Liu, M.; McGillicuddy, R. D.; Vuong, H.; Tao, S.; Slavney, A. H.; Gonzalez, M. I.; Billinge, S. J. L.; Mason, J. A. Network-Forming Liquids from Metal-Bis(Acetamide) Frameworks with Low Melting Temperatures. *J. Am. Chem. Soc.* **2021**, *143* (7), 2801–2811. https://doi.org/10.1021/JACS.0C11718.

(80) Tyumentsev, M. S.; Foreman, M. R. S. J.; Steenari, B. M.; Ekberg, C. Temperature Effect on the Distribution of Lanthanides(III) in the Perchlorate-Malonamide-Methyl Isobutyl Ketone Systems. *J. Chem. Thermodyn.* **2019**, *131*, 133–148. https://doi.org/10.1016/J.JCT.2018.10.021.

(81) Brigham, D.; Badajoz, C.; Cote, G.; Nash, K. L. Extraction of Trivalent Lanthanides and Americium by Tri-n-Octylphosphine Oxide from Ammonium Thiocyanate Media. *Solvent Extr. Ion Exch.* **2011**, *29* (2), 270–291. https://doi.org/10.1080/07366299.2011.556919.

(82) Choppin, G. R.; Bertrand, P. A.; Hasegawa, Y.; Rizkalla, E. N.; Hasegawa, Y. Thermodynamics of Complexation of Lanthanides by Benzoic and Isophthalic Acids. *Inorg. Chem.* **1982**, *21* (10), 3722–3724. https://doi.org/10.1021/IC00140A025.

(83) Choppin, G. R.; Dadgar, A.; Rizkalla, E. N. Thermodynamics of Complexation of Lanthanides by Dicarboxylate Ligands. *Inorg. Chem.* **1986**, *25* (20), 3581–3584. https://doi.org/10.1021/IC00240A009.

(84) Grimes, T. S.; Zalupski, P. R.; Martin, L. R. Features of the Thermodynamics of Trivalent Lanthanide/Actinide Distribution Reactions by Tri-n-Octylphosphine Oxide and Bis(2-Ethylhexyl) Phosphoric Acid. *J. Phys. Chem. B* **2014**, *118* (44), 12725–12733. https://doi.org/10.1021/JP507727V.

(85) Suresh, G.; Murali, M. S.; Mathur, J. N. Thermodynamics of Extraction of Am(III) and Eu(III) from Different Anionic Media with Tri-n-Octyl Phosphine Oxide. *Radiochim. Acta* **2003**, *91* (3), 127–134. https://doi.org/10.1524/RACT.91.3.127.19983.

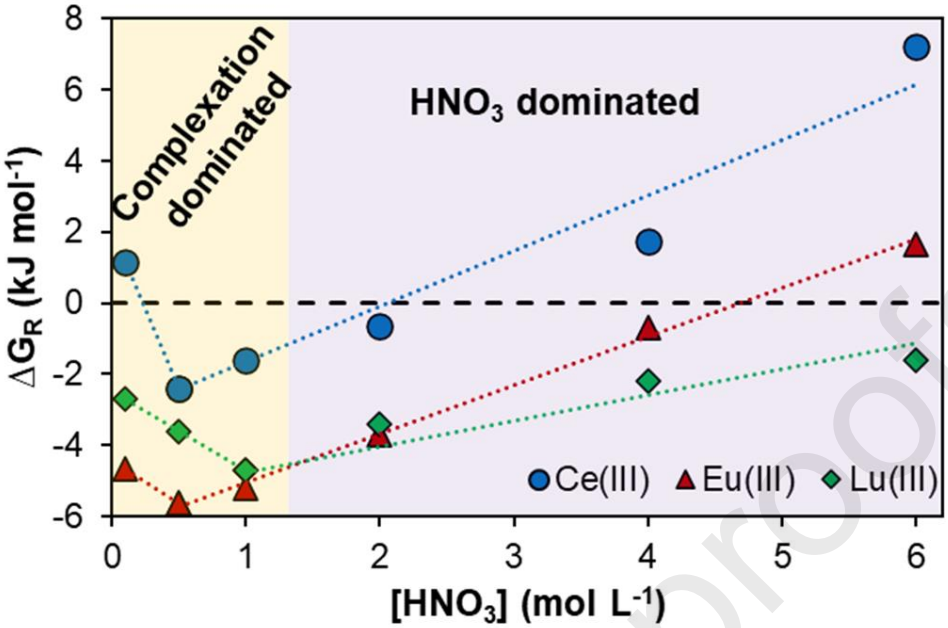

Highlights

- The hydrophobic eutectic solvent composed of trioctylphophine oxide (TOPO) and decanoic acid ($C_{10}OOH$) was applied to the extraction of lanthanides from HNO_3 solutions.
- Emphasis was placed on the determination of the relationship between the eutectic phase structuration and the extraction performance.
- A compromise between maximum Ln^{3+} loading and selectivity was observed.
- Ln^{3+} extraction is determined by the variation in the quantity of weakly hydrogen bonded TOPO ligands.
- Eutectic solvents appear as promising model solvents to explore the role of hydrogen bonding interactions in solvent extraction.

CRediT author statement

Ueslei G. Favero: Investigation, Writing- Original draft preparation. **Nicolas Schaeffer:** Writing- Original draft preparation, Supervision, Conceptualization. **Helena Passos:** Supervision. **Kaíque A.M.L. Cruz:** Investigation. **Duarte Ananias:** Investigation. **Sandrine Dourdain:** Investigation. **Maria C. Hespanhol:** Conceptualization, Funding acquisition, Supervision. All authors participated in the review and editing of this work.

Declaration of interests

☒The authors declare that they have no known competing financial interests or personal relationships that could have appeared to influence the work reported in this paper.

☐The authors declare the following financial interests/personal relationships which may be considered as potential competing interests: